The American Journal of Pathology, Vol. 174, No. 4, April 2009

DOI: 10.2353/ajpath.2009.080503

Neurobiology

Microtubule Depolymerization Suppresses α-Synuclein Accumulation in a Mouse Model of Multiple System Atrophy

Kimiko Nakayama, Yasuyo Suzuki, and Ikuru Yazawa

From the Laboratory of Research Resources, National Institute for Longevity Sciences, National Center for Geriatrics and Gerontology, Obu, Japan

Multiple system atrophy (MSA) is a neurodegenerative disease caused by an accumulation of α-synuclein (α-syn) in oligodendrocytes. Little is known about the cellular mechanisms by which α-syn accumulation causes neuronal degeneration in MSA. Our previous research, however, revealed that in a mouse model of MSA, oligodendrocytic inclusions of α-syn induced neuronal accumulation of α-syn, as well as progressive neuronal degeneration. Here we identify the mechanisms that underlie neuronal accumulation of α-syn in a mouse MSA model. We found that the α-syn protein binds to β-III tubulin in microtubules to form an insoluble complex. The insoluble α-syn complex progressively accumulates in neurons and leads to neuronal dysfunction. Furthermore, we demonstrated that the neuronal accumulation of insoluble α-syn is suppressed by treatment with a microtubule depolymerizing agent. The underlying pathological process appeared to also be inhibited by this treatment, providing promise for future therapeutic approaches. ***(Am J Pathol 2009, 174:1471–1480; DOI: 10.2353/ajpath.2009.080503)***

Important advances in hereditary neurodegenerative disorders have risen from research using molecular biology techniques. For example, identification of the genes responsible for familial Alzheimer's disease and hereditary polyglutamine diseases is among the most significant achievements in neuroscience.[1,2] In contrast, little progress has been made in research on the biology of neurodegeneration in a group of non-hereditary neurodegenerative disorders. Multiple system atrophy (MSA) is a non-hereditary neurodegenerative disease that is clinically characterized by autonomic nervous system failure as a symptom of Shy-Drager syndrome and Parkinsonism as a symptom of striatonigral degeneration.[3,4] The cellular mechanisms underlying the neurodegeneration are not understood, and no prospective therapeutic target for MSA has been presented.

Three significant neuropathological features characterize MSA histologically: glial cytoplasmic inclusions (GCIs), neuronal inclusions, and neuropil threads.[5] All three are composed of α-synuclein (α-syn). GCIs, the first neuropathological manifestation to be described, are oligodendrocytic inclusions.[6–8] Previous studies on GCIs reported that filaments isolated from the central nervous system (CNS) of patients with MSA were labeled by α-syn antibodies.[9] Accumulated α-syn comprises a major component of the inclusions in MSA[10,11] and might be the primary lesion that eventually compromises nerve cell function and viability in MSA.[12] However, the relevance of α-syn accumulation in oligodendrocytes to the neuronal degeneration in MSA was unknown.

No study had demonstrated that α-syn accumulation in oligodendrocytes leads to neuronal degeneration before the establishment of a mouse model of MSA. Three transgenic (Tg) mouse models in which human wild-type α-syn is overexpressed in CNS oligodendrocytes under the control of different promoters were generated.[13–15] Two of the three mouse lines showed that the accumulation of α-syn as GCIs leads to neuronal degeneration in the mouse CNS.[14,15]

Supported by the Ministry of Health, Labor and Welfare, Japan (the Research Grant for Longevity Sciences (18A-4) and a Grant-in-Aid for "the Research Committee for Ataxic Diseases" of the Research on Measures for Intractable Diseases), Grants-in-Aid (20700327) for Scientific Research from the Japan Society for the Promotion of Science, Japan Foundation for Aging and Health, Okinaka Memorial Institute for Medical Research, and the Life Science Foundation of Japan.

Accepted for publication January 5, 2009.

Supplemental material for this article can be found on *http://ajp.amjpathol.org.*

Address reprint requests to Ikuru Yazawa, MD, Ph.D., Laboratory of Research Resources, National Institute for Longevity Sciences, National Center for Geriatrics and Gerontology, 36-3 Gengo, Morioka-cho, Obu-shi, Aichi 474-7522, Japan. E-mail: yazawa@nils.go.jp.

Our previous study of the Tg mouse model demonstrated that the formation of GCI-like α-syn inclusions leads finally to neuronal degeneration, as exemplified by motor impairment in the phenotype, macroscopically apparent brain atrophy, and histologically decreased numbers of neurons with gliosis.[14] Thus, the accumulation of α-syn in oligodendrocytes induced the secondary neuronal degeneration, and we suggested that a similar disease process underlies MSA.

Here, we elucidated novel pathological mechanisms of neuronal accumulation of α-syn in the mouse model of MSA. We identified a protein, microtubule β-III tubulin, that interacts with α-syn and forms an insoluble protein complex. Moreover, the accumulation of α-syn is suppressed by inhibiting polymerization of microtubules. Important insights into MSA neurodegeneration and therapeutic targets have therefore emerged from this mouse model.

Materials and Methods

Primary Culture of Neurons and Glial Cells

Primary cultures of glial cells were obtained as previously described.[16] Briefly, glial cells were prepared from the brains of 1- to 3-day-old (P1-3) non-Tg and Tg mice. Cerebral hemispheres were mechanically disrupted. The cell suspensions were transferred to poly-L-lysine (20 μg/ml)-coated culture flasks (4 brains/75 cm^2 flask) and incubated in Dulbecco's modified Eagle's medium containing 10% fetal bovine serum supplemented with penicillin (50 U/ml), streptomycin (50 μg/ml), glutamine (1 mmol/L), and insulin (50 μg/ml, Sigma-Aldrich). Primary cultures of neuronal and glial cells were prepared from the brains of P0-P1 non-Tg and Tg mice. Cerebral cortices were dissected from mice and treated with 0.125% trypsin for 15 minutes at 37°C as previously described.[17] The dissociated cells were plated on 15 mm polyethylenimine (0.01%, Sigma-Aldrich)-coated glass coverslips (Matsunami, Japan) at a density of 2.4×10^5 cells/cm^2 for immunocytochemistry or 4.0×10^6 cells/cm^2 per polyethylenimine-coated 75 cm^2 flask for biochemical experiments. The cells were maintained in a 1:1 mixture of Dulbecco's modified Eagle's medium containing 10% fetal bovine serum and neurobasal medium with B27 supplement and penicillin (50 U/ml), streptomycin (50 μg/ml), glutamine (1 mmol/L), and insulin (50 μg/ml, Sigma-Aldrich). Half of the medium was replaced twice weekly. To inhibit proliferation of non-neuronal cells, after 4 days in culture, cytosine-1-β-D-arabinofuranoside (AraC, 0.5 μmol/L, Sigma-Aldrich) was added for 3 days. All chemicals for culture were purchased from Invitrogen, unless otherwise stated. To assay the effect microtubule function on α-syn, cultured cells were treated with 3 μmol/L nocodazole (Sigma-Aldrich) for 12 hours at DIV30 or 3 nmol/L nocodazole from DIV21. To enhance the spontaneous firing rate of cortical neurons, neurons cultured longer than DIV27 were treated with picrotoxin (PTX; 100 μmol/L, Wako, Japan), a blocker of gamma-aminobutyric acid A receptor/Cl channels.

Anti-α-Synuclein Antibodies

Syn204 is a monoclonal antibody raised against recombinant human α-syn, which selectively recognizes a human α-syn epitope between amino acid residues 87 and 110.[18] Anti-rat synuclein 1 (Syn-1; BD Bioscience) is a monoclonal antibody raised against rat α-syn that recognizes mouse α-syn. To generate an antibody specific to mouse α-syn, a synthetic peptide corresponding to mouse α-syn residues 115 to 125 (DMPVDPGSEAY) was conjugated with keyhole limpet hemocyanin, and used to immunize rabbits. The antisera were purified by affinity chromatography. The resulting polyclonal antibody, Syn-4469, was used for immunoreactive probing.

Immunocytochemistry

Neurons cultured on glass coverslips were fixed in 4% paraformaldehyde in PBS containing 4% sucrose for 15 minutes, and further fixed in methanol (−20°C) for 5 minutes. Neurons were then washed with PBS and blocked in PBS containing 2% bovine serum albumen and 2% goat serum for 2 hours at room temperature. Neurons were incubated with primary antibodies for 1 hour at room temperature in blocking solution. The primary antibodies used were 1:2000 Syn-1, 1:1000 mouse anti-CNPase (Lab Vision), 1:1000 mouse anti-MAP2 (Sigma-Aldrich), and 1:2000 anti-Tuj1 (Covance). After incubation with a primary antibody, the neurons were washed extensively in PBS and incubated for 20 minutes with fluorescent secondary antibody conjugates (goat anti-mouse- or goat anti-rabbit-Alexa488, 1:2000, or Alexa594, 1:2000; Molecular Probes). For cell counting, fixed cells were imaged using a microscope (Olympus, Japan) with ×10 objective lens and captured with a cooled CCD camera. Cells were manually counted in at least five fields for each series of experiments. In some of experiments, pyramidal neurons were confirmed by immunostaining with anti-MAP2 antibody. To assess cell density changes during culture, double positive cells with marker protein immunostaining and Hoechst 33258 were counted by using Metamorph software (Universal Imaging Corp.).

Biochemical Analysis of α-Synuclein Solubility

Proteins were extracted from the dissociated cultures as described above. Cultured cells were homogenized in 0.5 ml of high-salt (HS) buffer (50 mmol/L Tris, pH 7.4, 750 mmol/L NaCl, 20 mmol/L NaF, and 10 mmol/L EGTA with protease inhibitors) per flask of cells and centrifuged at 100,000 × *g* for 30 minutes; the supernatant was used as the HS-soluble fraction. The resulting pellet was further extracted with 10% sucrose and 50 mmol/L Tris, pH 7.6 to float and remove myelin and associated lipids. The pellets were dissolved in radioimmunoprecipitation (RIPA) buffer (50 mmol/L Tris, pH 8.0, 150 mmol/L NaCl, 5 mmol/L EGTA, 1% NP-40,

0.5% sodium deoxycholate, and 0.1% SDS) with protease inhibitors and centrifuged at 100,000 × g for 30 minutes at 4°C. The RIPA-soluble supernatant was used as the RIPA fraction. The pellets were extracted with 70% formic acid (FA) by sonication. Protein concentrations of HS and RIPA samples were determined using a BCA protein assay kit (Pierce). FA-extracted samples were dried and resuspended in SDS sample buffer. Equal amounts of samples were separated by SDS-polyacrylamide gel electrophoresis and transferred to PVDF membranes (ATTO, Japan). Membranes were blocked with 5% solution of powdered skimmed milk-0.3% Tween 20-Tris-buffered saline (50 mmol/L Tris, pH 7.4, 150 mmol/L NaCl), incubated with primary antibodies, followed with either goat anti-mouse or goat anti-rabbit antibody conjugated to horseradish peroxidase (Zymed), detected by an ECL plus system (GE), and exposed on X-ray film (Fujifilm, Japan). The protein levels were quantified using Image J software.

Immunoprecipitation

Homogenates were extracted as described above. The lysates were pre-cleared with protein G sepharose (Santa Cruz). Agarose-coupled mouse IgG was then added and incubated at 4°C for 2 hours. For the precipitation with α-syn, the immunocomplex was incubated with protein G Sepharose at 4°C overnight, and washed three times with RIPA buffer. Proteins were eluted from the beads by boiling in SDS sample buffer, and samples were subjected to immunoblotting.

Expressing Recombinant α-Synuclein and β-III Tubulin in COS-7

The complete cDNA sequences of the *Snca* and *Tubb3* genes were obtained by RT (reverse transcription)-PCR cloning using total RNA isolated from the brain of a 3-month-old non-Tg control mouse as a template. To fuse FLAG tag and c-Myc tag sequences to the 5′-region of *Snca* and *Tubb3* genes, respectively, PCR was performed using primers containing the tag sequence. The PCR products were subcloned into pT7Blue (Novagene). To express recombinant Snca and Tubb3, expression vectors were changed to pcDNA3.1(+) (Invitrogen) for COS-7 cells. COS-7 cells were maintained in Dulbecco's modified Eagle's medium supplemented with 10% fetal bovine serum. FuGENE 6 (Roche Applied Science) was used to introduce exogenous DNA into COS-7 cells according to the manufacturer's instructions. Briefly, 24 hours after cells were plated, each dish was transfected with *Snca*- or *Tubb3*-pcDNA3.1(+) and FuGENE, and incubated at 37°C for 48 hours. The sequences of the constructs were verified by an ABI 3100-Avant Genetic Analyzer.

Results

Increase in Amount and Insolubility of Endogenous Mouse α-Synuclein in Cultured Neurons Derived from Tg Mice

A previous study revealed that GCI-like inclusions of human α-syn in oligodendrocytes led to the age-dependent accumulation of endogenous mouse α-syn in neuronal axons and nerve terminals of the CNS of Tg mice over 6 months of age.[14] To elucidate the primary processes of the α-syn regulation and formation of insoluble accumulation in neurons, we prepared primary cultures of neurons and glial cells derived from non-Tg and Tg mice and compared the properties. First we confirmed the expression of human α-syn in oligodendrocytes. The cultured cells from 7 days *in vitro* (DIV7) to DIV35 were stained with Syn204, which specifically recognizes human α-syn. We detected Syn204-positive cells derived from only Tg mice (Figure 1A). The Syn204-positive cells

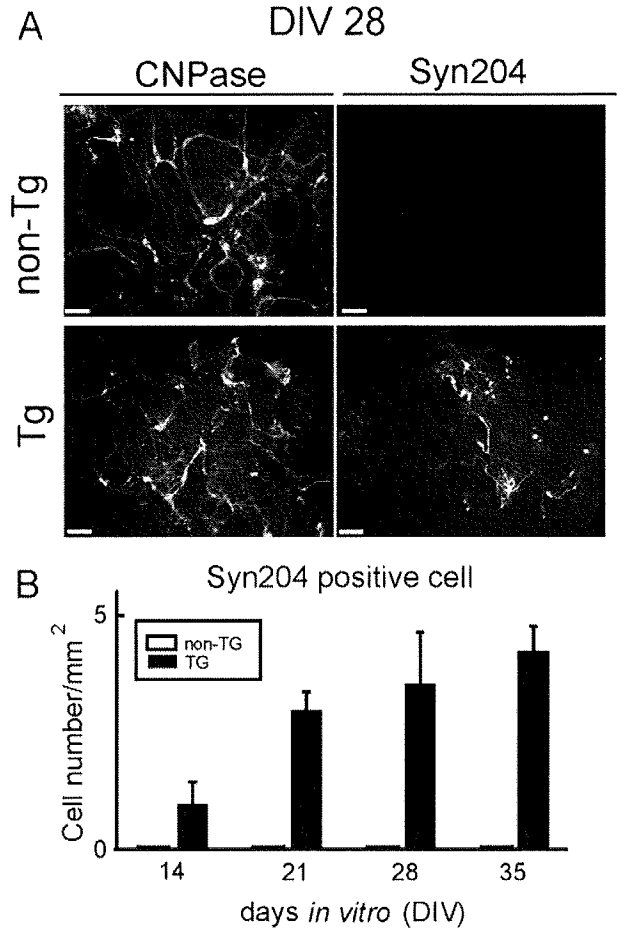

Figure 1. Human α-synuclein is overexpressed in cultured oligodendrocytes derived from Tg mice. **A:** Immunofluorescent staining of cultured oligodendrocytes for CNPase (**left**) and wild-type human α-syn (**right**) at DIV21. Cultured oligodendrocytes were derived from non-Tg and Tg mice. A Syn204-positive oligodendrocyte overexpressing human wild-type α-syn was observed in the cultured cells from Tg mice. Scale bar = 100 μm. **B:** Cell density of the oligodendrocytes overexpressing human wild-type α-syn was obtained by counting Syn204-positive cells over five objective fields in each series of cultures. Means data are plotted from three independent series of cultures. Data are presented as means ± SEM.

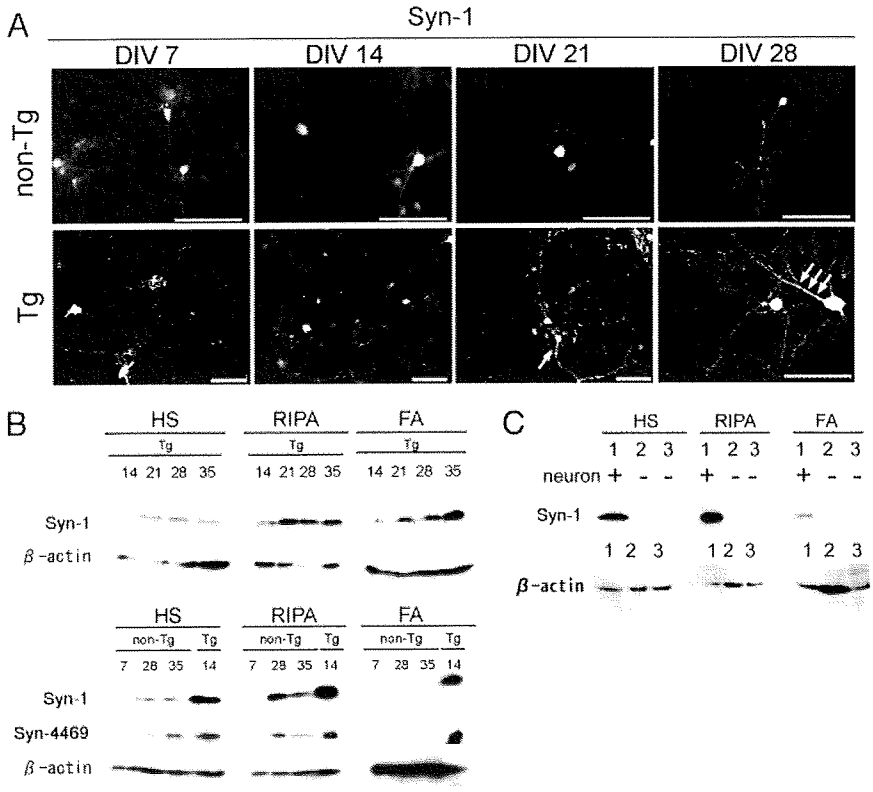

Figure 2. Increase in amount and insolubility of endogenous mouse α-syn in cultured neurons derived from Tg mice. **A:** Immunofluorescent staining for endogenous mouse α-syn in cultured cells from non-Tg and Tg mice. In Tg mouse cells, the protein expression level of mouse α-syn was increased and the distribution was predominantly diffuse in cell bodies and neurites (**arrows**). Scale bar = 100 μm. **B:** Immunoblots of cultured cells were stained with Syn-1, Syn-4469, and β-actin. Cultured neuronal and glial cells of Tg mice at DIV14, DIV21, DIV28, and DIV35, and those of non-Tg mice at DIV7, DIV28, and DIV35, were sequentially extracted with HS, RIPA, and FA. Insoluble α-syn was detected in the FA fraction of Tg mouse cells. Representative immunoblots of three independent experiments. **C:** Sequentially extracted samples of cultured neuronal and glial cells of Tg mice at DIV35 (lane 1), pure glial cells of non-Tg mice at DIV33 (lane 2), and pure glial cells of Tg mice at DIV33 (lane 3) were immunoblotted with Syn-1. α-Syn was detected in the fractions of Tg mouse neuronal and glial cells but not in the pure glial cells of non-Tg and Tg mice. Representative immunoblots of three independent experiments.

increased in number after DIV14 in Tg mice (black bar) (DIV14, 0.96 ± 0.64 cells/mm^2; DIV21, 2.97 ± 0.51 cells/mm^2; DIV28, 3.53 ± 1.44 cells/mm^2, DIV35, 4.33 ± 0.88 cells/mm^2), while no Syn204-positive cells were detected in non-Tg mice (white bar) (Figure 1B). In contrast, when the cultured cells were stained with anti-CNPase antibody (CNPase) as an oligodendrocyte marker, the cell densities of oligodendrocytes showed no significant difference between Tg and non-Tg mice (see supplemental Figure 1 at *http://ajp.amjpathol.org*). Next, we studied the expression of mouse α-syn in neurons cultured with glial cells using immunocytochemical methods. We generated an antibody, Syn-4469, which selectively recognizes mouse α-syn (see supplemental Figure 2 at *http://ajp.amjpathol.org*). In the Tg mouse cultured cells, Syn-4469 and Syn-1 showed the increased staining of mouse α-syn in neurons, which was clearly distinguished from the staining of over-expressing α-syn in oligodendrocytes (see supplemental Figure 3 at *http://ajp.amjpathol.org*). Mouse α-syn in the cultured cells of Tg and non-Tg mice was monitored by immunofluorescence from DIV7 to DIV35 using Syn-1, an antibody that recognizes mouse α-syn (Figure 2A). Cells from non-Tg mice from DIV7 to DIV35 showed synaptic enrichment similar to that observed in other presynaptic membrane proteins such as synaptophysin, as previously demonstrated in the literature.[19–22] In cells from Tg mice from DIV7 to DIV14, mouse α-syn is initially observed in neuronal cell bodies, and there was no difference in the expression level and intercellular distribution of mouse α-syn between in Tg and non-Tg mice. The protein had predominantly localized to presynaptic terminals and co-localized with synaptophysin by DIV14 (data not shown). At DIV21 and remarkably after DIV28 in Tg mice, however, a distinct increase in mouse α-syn was observed within the neuronal cell bodies and neurites in the CNS (Figure 2A, lower panels). In normal human brain extracts, α-syn was reported to be distributed almost entirely in the soluble cytosol fraction and detected in membrane fractions including those rich in vesicle and synaptic membranes, but it is also detected in the insoluble fraction in the MSA brain.[14,23] We biochemically analyzed the solubility of mouse α-syn in the cultured neurons from Tg mice by sequential extraction, as described in the Materials and Methods. Neuronal and glial cells of Tg and non-Tg mice cultured more than DIV7 were sequentially extracted with HS, RIPA, and FA buffers. Immunoblotting of the extracts staining with Syn-1 and Syn-4469 detected insoluble α-syn in FA fraction of cells from Tg mice cultured more than DIV14, but not in that from non-Tg mice (Figure 2B). The immunoblotting analysis showed that insoluble mouse α-syn progressively increased with the increase in the number of days *in vitro* (see supplemental Figure 4 at *http://ajp.amjpathol.org*). To examine whether the insoluble α-syn was mouse α-syn in neurons of Tg mice, we examined pure cultures of glial cells of Tg and non-Tg mice. Syn-1 detected no immunoreactivity on the immunoblots of fractions of the pure cultures of Tg and non-Tg glial cells (Figure 2C). The results revealed that insoluble mouse α-syn was increased in the neurons but not in the oligodendrocytes of Tg mice. Thus, the histological and biochemical data together indicated that insoluble mouse α-syn was accumulated in cultured neurons derived from Tg mice.

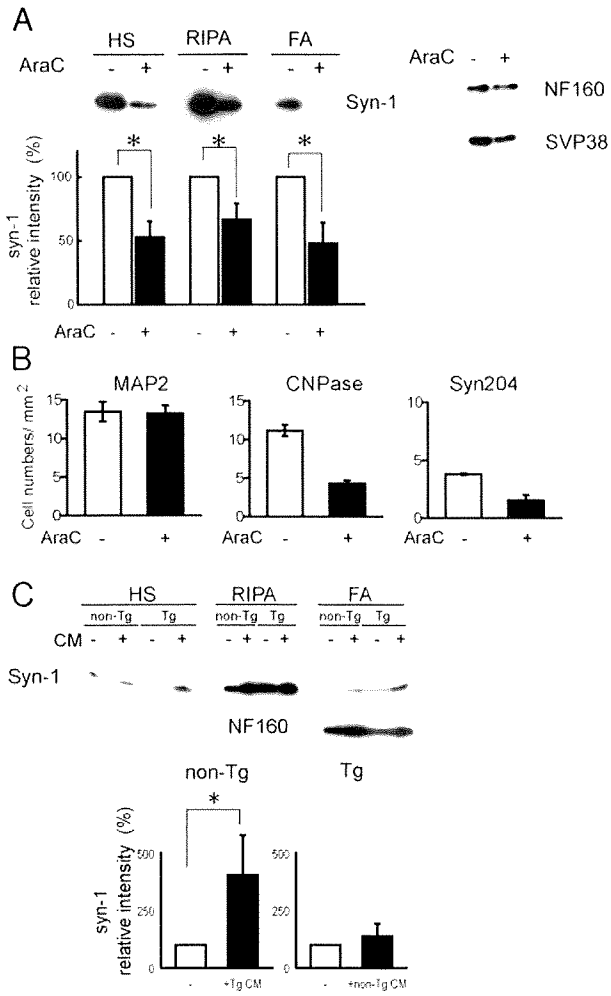

Figure 3. Effects of oligodendrocytes overexpressing human α-syn on neurons. **A:** Cells of Tg mice at DIV30 cultured with (+) and without (−) AraC were sequentially extracted. The immunoblots were stained with Syn-1 and antibodies to 160 kDa-neurofilament (NF160) and anti-synaptophisin (SVP38), and only the immunoblots probed with Syn-1 showed that expression of α-syn was decreased by the AraC treatment. α-Syn expression on the immunoblots of Tg mouse cultures with (closed bars) and without AraC (open bars) was quantitated. All α-syn signals were normalized to the signal for NF160 to account for the amount of neuronal protein loaded per lane. HS, 52.8± 12.4%; RIPA, 66.5± 12.7%; FA, 48.0± 16.1%, five series of cultures. $^*P < 0.01$. Data are presented as means ± SEM. **B:** Bar graphs comparing the number of MAP2 positive cells (neurons), CNPase-positive cells (oligodendrocytes), and syn204-positive cells of Tg mouse cultures with (closed bars) and without AraC (open bars) ($n = 3$). Data are presented as means ± SEM. **C:** At DIV30, cultured cells of non-Tg mice treated with conditioned media (CM) from Tg mouse cell cultures and those of Tg mice treated with conditioned media derived from non-Tg mouse cell cultures were sequentially extracted, and the immunoblots were stained with Syn-1 and NF160. The FA fractions of α-syn were quantified on the immunoblots of non-Tg and Tg mouse cultures with (closed bars) and without (open bars) conditioned media ($n = 3$). Note that insoluble α-syn was detected in FA fraction of non-Tg mouse treated with the conditioned media of Tg mouse cells. Data are presented as means ± SEM. $^*P < 0.05$ (Mann-Whitney *U*-test).

Oligodendrocytic Inclusions Induce Neuronal Accumulation of Insoluble Mouse α-Synuclein

To confirm that the oligodendrocytes in which human α-syn was overexpressed caused the increase of mouse α-syn in the neurons of Tg mice, we treated the neuronal and glial cell cultures with cytosine-1-β-D-arabinofuranoside (AraC; 0.5 μmol/L) for three days after DIV7 to inhibit proliferation of glial cells. When examined microscopically, the number of glial cells, including oligodendrocytes, was reduced in the culture. The immunoblotting analysis showed that the mouse α-syn expression was decreased by the treatment with AraC (HS, 52.8 ± 12.43%; RIPA, 66.5 ± 12.65%; FA, 48.0 ± 16.1%), although 160-kDa neurofilament and synaptophisin expressions showed no change due to the treatment (Figure 3A). The cell density of MAP2-positive neurons showed no significant difference between cultured neurons with and without AraC. The CNPase-positive and Syn204-positive oligodendrocytes decreased in number by the treatment with AraC (Figure 3B). Next, we investigated how oligodendrocytic accumulation of human α-syn causes neuronal accumulation of insoluble mouse α-syn. Non-Tg mouse cells after DIV14 were treated with conditioned media derived from Tg mouse cell cultures and vice versa. The immunoblots of sequentially extracted cultured cells showed that the insoluble α-syn was detected in the FA fraction of non-Tg mouse treated with Tg mouse conditioned media. No remarkable difference was detected between the FA fractions of Tg mouse cell cultured with and without non-Tg conditioned media (non-Tg mice: FA, 404.1 ± 172.3%; Tg mice: FA, 138.2 ± 54.1%) (Figure 3C). The result indicates that the conditioned media of Tg mouse cell cultures contained oligodendrocyte-derived signals that induced neuronal α-syn accumulation. Thus, it was the oligodendrocytic accumulation of α-syn that induced accumulation of insoluble α-syn in the Tg mouse neurons.

α-Synuclein Binds to β-III Tubulin and Forms Insoluble Protein Complex

We next addressed the mechanism by which the accumulation of insoluble α-syn causes neuronal degeneration in Tg mice. We investigated which proteins interact with α-syn in Tg mice. First, we tried to identify the proteins that change the soluble fraction to an insoluble one on the immunoblots of the sequentially extracted samples from Tg mice. We found that neuron-specific β-III tubulin antibody (Tuj1) labeled a band in the insoluble fractions on the immunoblots of the Tg mouse cells, but showed no immunoreactivity to the cell fractions of non-Tg mice (Figure 4A). The other neuronal proteins showed no difference in solubility between Tg and non-Tg mice. Second, we evaluated the interaction between α-syn and β-III tubulin by immunoprecipitation analysis. The analysis showed that β-III tubulin was co-immunoprecipitated with mouse α-syn in the RIPA fraction of Tg mouse cells (Figure 4B). No other β-tubulin isoforms was co-immunoprecipitated. Third, double-labeling immunofluorescent staining of Tg mouse cells showed that mouse α-syn was colocalized with β-III tubulin in the neurites and neuronal cell bodies (Figure 4C). The cell density of Tuj1-positive neurons showed no significant difference between Tg and non-Tg mice (see supplemental Figure 5 at *http://ajp.amjpathol.org*). These data demonstrate that the increase of mouse α-syn expression in neurites and cell bodies caused binding of the α-syn with β-III tubulin to

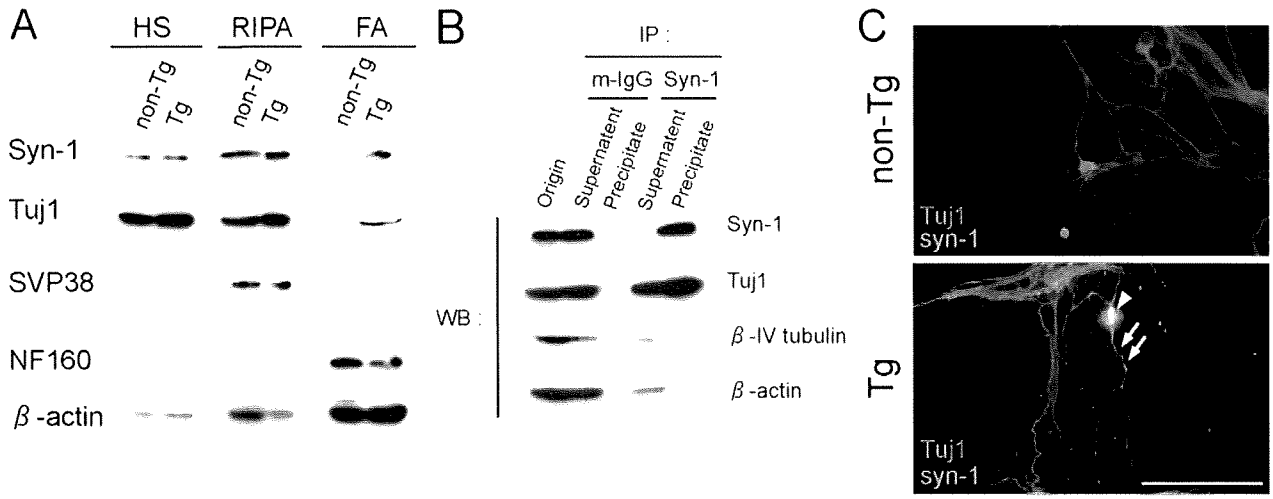

Figure 4. Protein-protein interaction of α-syn and β-III tubulin in Tg mice. **A:** Cultured neuronal and glial cells of Tg and non-Tg mice at DIV33 were sequentially extracted with HS, RIPA, and FA. The immunoblots were stained by Syn-1, Tuj1, β-actin as a protein marker, and SVP38 (anti-synaptophisin antibody) as a neuronal protein marker. Insoluble β-III tubulin was detected in the same FA fraction of Tg mice as the insoluble α-syn on the immunoblots of Tg mouse cells. Representative immunoblots of three independent experiments. **B:** Association of α-syn and β-III tubulin in RIPA fraction of Tg mouse cells was examined by immunoprecipitation with Syn-1 or mouse IgG as a negative control antibody, followed by immunoblotting with Syn-1, Tuj1, β-IV tubulin, or β-actin. β-III tubulin was co-immunoprecipitated with mouse α-syn. **C:** Double-labeling immunofluorescent staining using antibodies Syn-1 to mouse α-syn (green) and Tuj1 to β-III tubulin (red) shows that α-syn colocalizes with β-III tubulin in the neurites (**arrows**) and neuronal cell bodies (**arrowhead**) derived from Tg mice (yellow). Scale bar = 100 μm.

form an insoluble complex. To verify that direct binding of the α-syn with β-III tubulin causes formation of the insoluble complex, COS-7 cells were transfected with *Snca*, *Tubb3*, or cotransfected with *Snca* and *Tubb3* respectively. The recombinant proteins expressed in COS-7 cells were sequentially extracted. The insoluble α-syn was detected in the FA fraction only in the COS-7 cells cotransfected with *Snca* and *Tubb3* (Figure 5A). Then, we evaluated the direct interaction between the recombinant α-syn and β-III tubulin by immunoprecipitation analysis (Figure 5B). We concluded that the direct binding of α-syn with β-III tubulin caused formation of the insoluble complex.

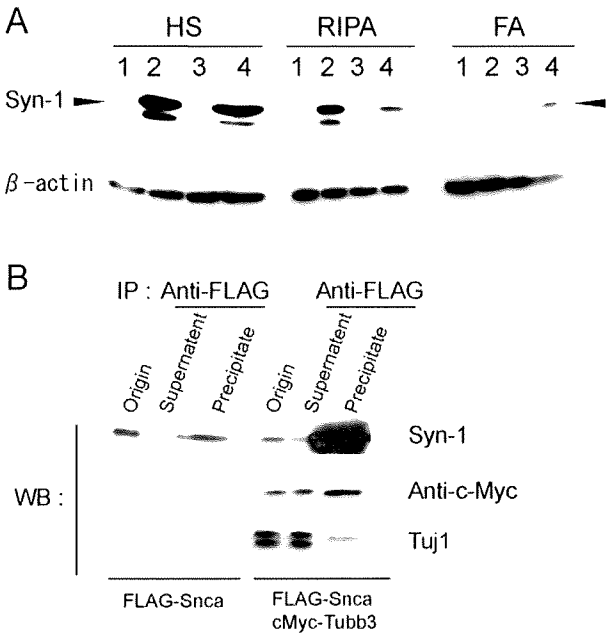

Figure 5. Direct binding of α-syn with β-III tubulin causes to form insoluble complex. **A:** COS-7 cells were transfected with the mock (lane 1), *Snca* (lane 2), *Tubb3* (lane 3), or cotransfected with *Snca* and *Tubb3* (lane 4). The recombinant proteins expressed by COS-7 were sequentially extracted. The immunoblots stained with Syn-1 showed that insoluble α-syn in the FA fraction was detected only in the COS-7 cells cotransfected with *Snca* and *Tubb3* (arrowhead). **B:** COS-7 cells were transfected with *FLAG-Snca*, or cotransfected with *FLAG-Snca* and *cMyc-Tubb3* for immunoprecipitation analysis. The fusion proteins expressed were immunoprecipitated with anti-FLAG antibody using anti-FLAG-agarose affinity gels, and the immunoblots of the immunoprecipitates were stained with Syn-1, anti-cMyc antibody, and Tuj1. The recombinant α-syn directly bound to the recombinant β-III tubulin.

Accumulation of Insoluble α-Synuclein Is Suppressed by Depolymerization of Microtubules

Because microtubule β-III tubulin binds α-syn and the insoluble protein complex thus formed accumulates in neurons, it was hypothesized that the accumulation of insoluble α-syn might be controlled by blocking microtubule polymerization in Tg mice. We investigated the effect of treatment with nocodazole, a microtubule-depolymerizing agent (3 μmol/L), on the accumulation of α-syn. Primary cultured cells of Tg and non-Tg mice were treated with nocodazole for 12 hours at DIV30 and sequentially extracted for immunoblotting (Figure 6A). Although soluble α-syn decreased in non-Tg mouse cells after nocodazole treatment, the soluble and insoluble α-syn in Tg mouse cells showed no difference after this treatment (non-Tg mice: HS, 41.6 ± 16.3%; RIPA, 65.0 ± 25.5%; Tg mice: HS, 89.9 ± 9.32%; RIPA, 100.2 ± 5.1%, FA, 96.8 ± 17.6%) (Figure 6B). The data indicate that microtubules play an important role in the regulation of α-syn in non-Tg mice. The accumulation of α-syn in Tg mice was not inhibited by nocodazole when it had already accumulated and formed the insoluble protein complex. Then we investigated whether nocodazole

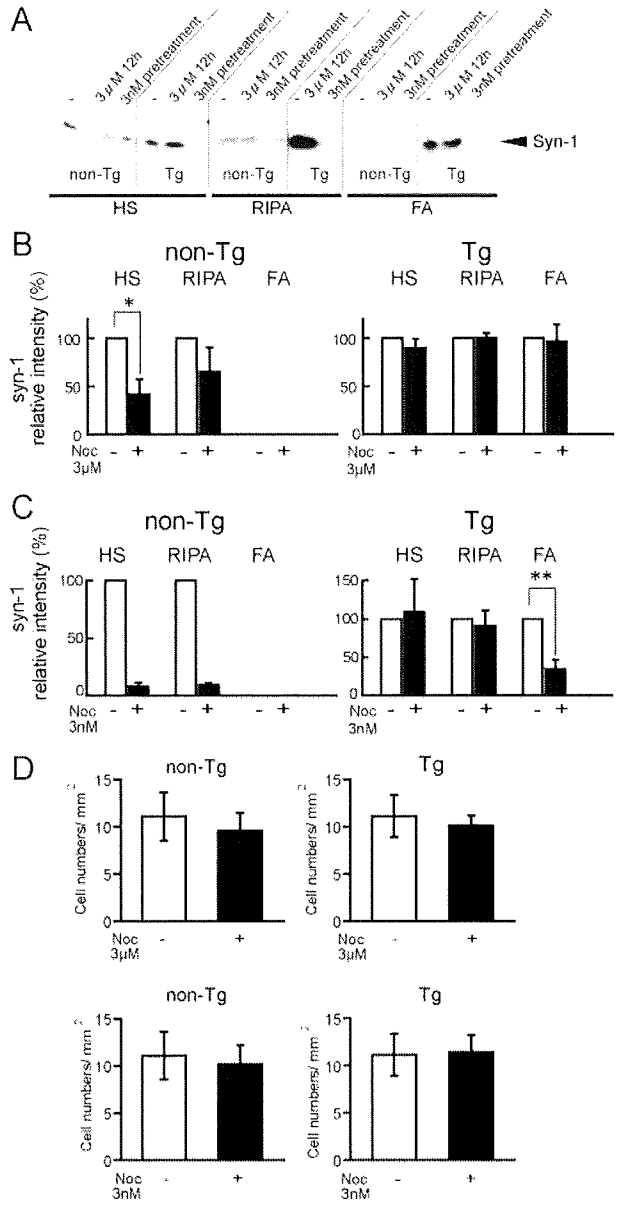

Figure 6. Effect of microtubule-depolymerizing agent on accumulation of insoluble α-syn. **A:** Cultured neuronal and glial cells from non-Tg and Tg mice were treated with (+) and without (−) nocodazole, and they were sequentially extracted at DIV30 ($n = 3$). The cells were treated with 3 μmol/L nocodazole at DIV30 for 12 hours (3 μM 12 h) and with 3 nmol/L nocodazole from DIV21 to DIV30 for 10 days (3nM pretreatment). Representative immunoblots of three independent experiments. **B:** Quantitative analyses of α-syn on the immunoblots of non-Tg and Tg mouse cultures with (closed bars) and without (open bars) treatment of 3 μmol/L nocodazole for 12 hours at DIV30. Soluble α-syn decreased in non-Tg mouse cells, whereas soluble and insoluble α-syn showed no difference in Tg mouse cells with the treatment. All α-syn signals are normalized to the signals for synaptophisin (SVP38; anti-synaptophisin antibody) to account for the amount of neuronal protein loaded per lane. $^*P < 0.05$. Data are presented as means ±SEM. **C:** Quantitative analyses of α-syn on the immunoblots of non-Tg and Tg mouse cultures with (closed bars) and without (open bars) pretreatment with 3 μmol/L nocodazole for 10 days. Insoluble α-syn was significantly reduced in the FA fraction of Tg mice by the pretreatment with nocodazole. All α-syn signals were normalized to the signal for synaptophisin (SVP38) to account for the amount of neuronal protein loaded per lane. $^{**}P < 0.01$. Data are shown as means ± SEM. **D:** Neuronal densities of non-Tg and Tg mouse cultures with (closed bars) and without (open bars) pretreatment with 3 μmol/L nocodazole for 12 hours and 3 nmol/L for 10 days were obtained by counting Hoechst 33258 and MAP2 double-positive cells over five objective fields in each series of cultures. Means data are plotted from three independent series of cultures.

treatment prevented the accumulation of α-syn in Tg mice before soluble α-syn starts to form an insoluble protein complex. Primary cultured cells from Tg mice were treated with nocodazole (3 nmol/L) from DIV20 to DIV30 and then sequentially extracted at DIV30 (Figure 6A). The immunoblotting analysis showed that the accumulation of α-syn decreased in Tg mouse cells with nocodazole pretreatment (non-Tg mice: HS, 7.89 ± 3.47%; RIPA, 9.52 ± 1.56%; Tg mice: HS, 109.2 ± 42.5%; RIPA, 90.6 ± 20.7%, FA, 34.5 ± 12.1%) (Figure 6C). The cell density of MAP2-positive neurons showed no significant difference between cultured neurons with and without nocodazole (Figure 6D). The data demonstrated that microtubule depolymerization suppressed the accumulation of insoluble α-syn in Tg mice. Therefore, the binding of α-syn to microtubules and formation of an insoluble protein complex induced the accumulation of α-syn, and it could be suppressed before the insoluble complex was formed.

Effect of Neuronal Function on Insoluble α-Synuclein Accumulation

Despite the accumulation and insolubilization of α-syn in neurons, we didn't find that the accumulation has a direct effect on whether or not the neurons will degenerate during cultured period. However we previously reported that progressive neuronal degeneration was accompanied in Tg mice after the sixth month. It is possible that the accumulation and insolubilization of α-syn in neurons affect the neuronal function and cause neuronal dysfunction. Because the localization of multiple synaptic proteins, including α-syn was modulated by activity dependent manner,[24] we examined whether neuronal activity affects the accumulation of α-syn in neuronal and glial cell cultures. The cultured cells were treated with picrotoxin (PTX; 100 μmol/L), a gamma-aminobutyric acid A receptor/Cl channel blocker, for 3 days from DIV27 to DIV30, and the proteins were sequentially extracted. Although non-Tg mouse cells showed a decrease in soluble α-syn with PTX treatment (Figure 7A), Tg mouse cells showed no difference in either soluble or insoluble α-syn with PTX treatment (Figure 7B). The cell density of MAP2-positive neurons showed no significant difference between cultured neurons with and without PTX (Figure 7C). The data showed that the modulation of α-syn by neuronal activity was disturbed in Tg mice and that the disturbance may accelerate the accumulation of α-syn.

Discussion

We previously reported that progressive neuronal degeneration was accompanied by neuronal accumulation of mouse α-syn in Tg mice overexpressing human α-syn in oligodendrocytes.[14] Although the accumulation of α-syn in neurons plays an important role in neuronal degeneration, the primary cellular process underlying the neuronal degeneration was not understood. The present study provides novel evidence that endogenous mouse α-syn,

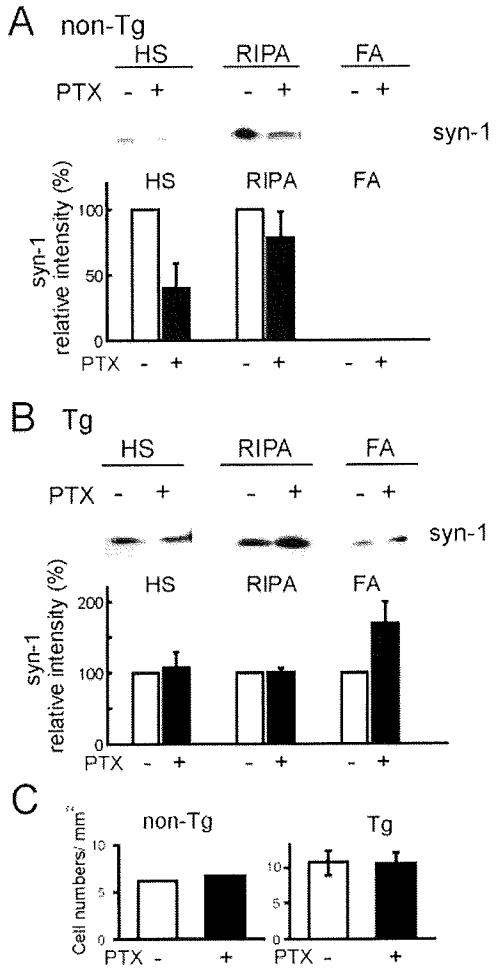

Figure 7. Neuronal activity controls accumulation of α-syn. Cells of non-Tg (**A**) and Tg (**B**) mice at DIV30 cultured with (+) and without (−) PTX were sequentially extracted. Although soluble α-syn decreased in non-Tg mouse cells after PTX treatment, the accumulation of α-syn showed no difference in Tg mouse cells with PTX treatment (n = 5). Bar graphs show quantitative analyses of α-syn expression on the immunoblots with (closed bars) and without (open bars) PTX in non-Tg (**A**) and Tg (**B**) mice. All α-syn signals were normalized to the signal for NF160 to account for the amount of neuronal protein loaded per lane (non-Tg mice: HS, 39.63± 19.34%; RIPA, 78.35± 19.50%; Tg mice: HS, 106.95± 22.24%; RIPA, 100.60± 6.09%; FA, 168.73± 30.61%, two series of cultures). **C:** Neuronal cell densities were obtained by counting Hoechst 33258 and MAP2 double positive cells over five objective fields in each series of cultures. Means data are plotted from two independent series of cultures.

which is increased by the formation of oligodendrocytic inclusions, binds to β-III tubulin in microtubules. The insoluble complex is progressively accumulated in neurons, leading to neuronal dysfunction in the Tg mouse model of MSA. Moreover, we demonstrated that the accumulation of the insoluble α-syn complex is suppressed by treatment with a microtubule depolymerizing agent. The results indicate that the binding of α-syn to β-III tubulin is a key process in the development of neuronal degeneration in the MSA mouse model.

One pathological process underlying the accumulation of α-syn in MSA is the accumulation of an insoluble protein complex in neurons induced by the binding of α-syn with β-III tubulin. We identified the microtubule component β-III tubulin as the protein that specifically interacts with α-syn in the Tg mice. Previous studies showed that β-tubulin is located in GCIs in the brain tissue of patients with MSA.[8,25,26] Ultrastructural studies demonstrated that GCIs were composed of oligodendrocytic microtubules with diameters of 20 to 30 nm.[25] Immunoelectron microscopy showed that α-syn positive inclusions in neuronal nuclei and oligodendrocytes of MSA were composed by bundles of filaments with a diameter of 10 to 20 nm.[27] Our previous observation of aged Tg mice with motor impairment demonstrated the distinct axonal accumulation of α-syn and the formation of α-syn inclusions in the degenerating axons and axonal terminals.[14] The axonal terminal inclusions were ultrastructurally composed of disordered tubular structures with diameters of approximately 20 to 35 nm.[14] The present data reveal that the formation and accumulation of insoluble complexes of α-syn and β-III tubulin is an important disease process in the neuronal dysfunction of an MSA mouse model. β-tubulin was reported to be co-immunoprecipitated with α-syn in normal human brain extracts.[27,28] We revealed no evidence of directly binding to the other β-tubulin isoforms. Although the physiological role of the interaction between α-syn and β-tubulin is not completely clear, previous reports showed that α-syn interacted with heterodimeric tubulin[28] and that tubulin initiated and promoted α-syn fibril formation under physiological conditions *in vitro*.[29] Indeed, in the MSA Tg mice, once the insoluble complex was formed, microtubule depolymerization agent was ineffective in blocking of the α-syn accumulation. However, microtubule depolymerization agent suppressed the accumulation of insoluble α-syn complex before the neuronal α-syn expression was developed by the oligodendrocytes overexpressing human α-syn. We plan to test the hypothesis that the regulation of insoluble α-syn complexes by the treatment is a therapeutic target for MSA. Because the microtubule depolymerizing agent blocks microtubule conformation and prevents microtubule function, the potential use can be toxic. There may be several approaches to inhibition of the accumulation of α-syn. Although the pathological mechanisms are not fully understood in MSA, this study could contribute to development of a therapeutic strategy against MSA neuronal degeneration.

Another pathological process that underlies the neuronal degeneration in MSA is the increase in the expression of α-syn in neurons due to the formation of GCIs in oligodendrocytes. We here demonstrated that insoluble α-syn accumulated in neuronal cell bodies and neurites after DIV21 in Tg mice. DIV21 is the crucial time at which the GCI-like inclusions start to develop in oligodendrocytes. Inhibition of glial cell proliferation by treatment with AraC prevented the accumulation of insoluble α-syn in Tg mouse neurons. Because reciprocal communication between neurons and oligodendrocytes is essential for the development of the CNS,[30] our study suggested that degenerated oligodendrocytes might regulate α-syn protein expression in neurons. Moreover, we demonstrated that conditioned media derived from Tg mouse cell cultures induced insoluble α-syn in non-Tg mouse cell cultures, suggesting abnormal regulation of α-syn due to the formation of GCI-like inclusions. We speculate

that abnormal regulation of neuronal α-syn expression by degenerated oligodendrocytes may trigger the onset of MSA.

Modulation and physiological function of α-syn by neuronal activity is disturbed in an MSA mouse model. Our present finding reveals that α-syn decreased in non-Tg mouse cells in response to neuronal activity due to PTX treatment, whereas the α-syn accumulation in response to neuronal activity due to PTX treatment showed no difference in Tg mouse cells. Neuronal activity controls the synaptic accumulation of α-syn, and α-syn disperses from the nerve terminal in response to neuronal activity.[24] Although steady-state levels of α-syn in non-Tg mouse cells are balance between production and clearance, the regulation of α-syn is disturbed in Tg mouse neurons due to the binding with β-III tubulin and formation of the insoluble complex. Because α-syn localizes to nerve terminals,[20,21,31] when expressed at physiological levels, it functions as a regulator of synaptic vesicle fusion and neurotransmitter release at the synapse.[32] The total number of vesicle fusion events in cell α-syn-overexpressing mice was significantly decreased.[33] Because endogenous mouse α-syn expression was increased in the presynaptic terminals of Tg mouse neurons,[14] the total number of synaptic vesicle fusion events may be significantly decreased. Therefore, it is hypothesized that the insolubility of α-syn causes abnormal α-syn synaptic accumulation, resulting to disturb the normal function of α-syn and age-dependent progressive neuronal degeneration. We expect to evaluate the synaptic function in Tg mice by electrophysiological approach.

Acknowledgments

We thank Virginia Lee and John Trojanowski for reading the manuscript and providing the MSA Tg mice, and Ryogen Sasaki for technical assistance.

References

1. Goedert M, Spillantini MG: A century of Alzheimer's disease. Science 2006, 314:777–781
2. Yazawa I: Pathological mechanism of neurodegeneration in polyglutamine diseases. Recent Research Developments in Biophysics and Biochemistry, vol 3. edited by SG Pandalai. India, Research Signpost, 2003, pp 21–28.
3. Graham JG, Oppenheimer DR: Orthostatic hypotension and nicotine sensitivity in a case of multiple system atrophy. J Neurol Neurosurg Psychiatry 1969, 32:28–34
4. Gilman S, Low PA, Quinn N, Albanese A, Ben-Shlomo Y, Fowler CJ, Kaufmann H, Klockgether T, Lang AE, Lantos PL, Litvan I, Mathias CJ, Oliver E, Robertson D, Schatz I, Wenning GK: Consensus statement on the diagnosis of multiple system atrophy. J Neurol Sci 1999, 163:94–98
5. Lowe JS, Leigh N: Disorders of movement and system degeneration. Greenfield's Neuropathology, vol 1, ed 2. Edited by DI Graham and PL Lantos. London Hodder Arnold, 2002, pp 343–346
6. Papp MI, Kahn JE, Lantos PL: Glial cytoplasmic inclusions in the CNS of patients with multiple system atrophy (striatonigral degeneration, olivopontocerebellar atrophy and Shy-Drager syndrome). J Neurol Sci 1989, 94:79–100
7. Arima K, Ueda K, Sunohara N, Arakawa K, Hirai S, Nakamura M, Tonozuka-Uehara H, Kawai M: NACP/ α-synuclein immunoreactivity in fibrillary components of neuronal and oligodendroglial cytoplasmic inclusions in the pontine nuclei in multiple system atrophy. Acta Neuropathol (Berl) 1998, 96:439–444
8. Tu PH, Galvin JE, Baba M, Giasson B, Tomita T, Leight S, Nakajo S, Iwatsubo T, Trojanowski JQ, Lee VM-Y: Glial cytoplasmic inclusions in white matter oligodendrocytes of multiple system atrophy brains contain insoluble α–synuclein. Ann Neurol 1998, 44:415–422
9. Spillantini MG, Crowther RA, Jakes R, Cairns NJ, Lantos PL, Goedert M: Filamentous α-synuclein inclusions link multiple system atrophy with Parkinson's disease and dementia with Lewy bodies. Neurosci Lett 1998, 251:205–208
10. Spillantini MG, Goedert M: The α-synucleinopathies: parkinson's disease, dementia with Lewy bodies, and multiple system atrophy. Ann NY Acad Sci 2000, 920:16–27
11. Duda JE, Lee VM-Y, Trojanowski JQ: Neuropathology of synuclein aggregates. J Neurosci Res 2000, 61:121–127
12. Goedert M: Alpha-synuclein and neurodegenerative diseases. Nat Rev Neurosci 2001, 2:492–501
13. Kahle PJ, Neumann M, Ozmen L, Muller V, Jacobsen H, Spooren W, Fuss B, Mallon B, Macklin WB, Fujiwara H, Hasegawa M, Iwatsubo T, Kretzschmar HA, Haass C: Hyperphosphorylation and insolubility of α-synuclein in transgenic mouse oligodendrocytes. EMBO Rep 2002, 3:583–588
14. Yazawa I, Giasson BI, Sasaki R, Zhang B, Joyce S, Uryu K, Trojanowski JQ, Lee VM-Y: Mouse model of multiple system atrophy: α-synuclein expression in oligodendrocytes causes glial and neuronal degeneration. Neuron 2005, 45:847–859
15. Shults CW, Rockenstein E, Crews L, Adame A, Mante M, Larrea G, Hashimoto M, Song D, Iwatsubo T, Tsuboi K, Masliah E: Neurological and neurodegenerative alterations in a transgenic mouse model expressing human α-synuclein under oligodendrocyte promoter: implications for multiple system atrophy. J Neurosci 2005, 25: 10689–10699
16. Richter-Landsberg C, Heinrich M: OLN-93: a new permanent oligodendroglia cell line derived from primary rat brain glial cultures. J Neurosci Res 1996, 45:161–173
17. Nakayama K, Kiyosue K, Taguchi T: Diminished neuronal activity increases neuron-neuron connectivity underlying silent synapse formation and the rapid conversion of silent to functional synapses. J Neurosci 2005, 25:4040–4051
18. Giasson BI, Jakes R, Goedret M, Duda JE, Leight S, Trojanowski JQ, Lee VM-Y: A panel of epitope-specific antibodies detects protein domains distributed throughout human α-synuclein in Lewy bodies of Parkinson's disease. J Neurosci Res 2000, 59:528–533
19. Maroteaux L, Scheller RH: The rat brain synucleins; family of proteins transiently associated with neuronal membrane. Brain Res Mol Brain Res 1991, 11:335–343
20. Jakes R, Spillantini MG, Goedert M: Identification of two distinct synucleins from human brain. FEBS Lett 1994, 345:27–32
21. Iwai A, Masliah E, Yoshimoto M, Ge N, Flanagan L, de Silva HA, Kittel A, Saitoh T: The precursor protein of non-A beta component of Alzheimer's disease amyloid is a presynaptic protein of the central nervous system. Neuron 1995, 14:467–475
22. Hsu LJ, Mallory M, Xia Y, Veinbergs I, Hashimoto M, Yoshimoto M, Thal LJ, Saitoh T, Masliah E: Expression pattern of synucleins (non-A beta component of Alzheimer's disease amyloid precursor protein/ α-synuclein) during murine brain development. J Neurochem 1998, 71:338–344
23. Dickson DW, Liu W, Hardy J, Farrer M, Mehta N, Uitti R, Mark M, Zimmerman T, Golbe L, Sage J, Sima A, D'Amato C, Albin R, Gilman S, Yen SH: Widespread alterations of α-synuclein in multiple system atrophy. Am J Pathol 1999, 155:1241–1251
24. Fortin DL, Nemani VM, Voglmaier SM, Anthony MD, Ryan TA, Edwards RH: Neural activity controls the synaptic accumulation of α-synuclein. J Neurosci 2005, 25:10913–10921
25. Nakazato Y, Yamazaki H, Hirato J, Ishida Y, Yamaguchi H: Oligodendroglial microtubular tangles in olivopontocerebellar atrophy. J Neuropathol Exp Neurol 1990, 49:521–530
26. Abe H, Yagishita S, Amano N, Iwabuchi K, Hasegawa K, Kowa K: Argyrophilic glial intracytoplasmic inclusions in multiple system atrophy: immunocytochemical and ultrastructural study. Acta Neuropathol (Berl) 1992, 84:273–277
27. Lin WL, DeLucia MW, Dickson DW: α-Synuclein immunoreactivity in neuronal nuclear inclusions and neurites in multiple system atrophy. Neurosci Lett 2004, 354:99–102

28. Payton JE, Perrin RJ, Clayton DF, George JM: Protein-protein interactions of alpha-synuclein in brain homogenates and transfected cells. Brain Res Mol Brain Res 2001, 95:138–145
29. Alim MA, Hossain MS, Arima K, Takeda K, Izumiyama Y, Nakamura M, Kaji H, Shinoda T, Hisanaga S, Ueda K: Tubulin seeds α-synuclein fibril formation. J Biol Chem 2002, 277:2112–2117
30. Simons M, Trajkovic K: Neuron-glia communication in the control of oligodendrocyte function and myelin biogenesis. J Cell Sci 2006, 119:4381–4389
31. Withers GS, George JM, Banker GA, Clayton DF: Delayed localization of synelfin (synuclein. NACP) to presynaptic terminals in cultured rat hippocampal neurons Brain Res Dev Brain Res 1997, 99:87–94
32. Gitler AD, Shorter J: Prime time for α-synuclein. J Neurosci 2007, 27:2433–2434
33. Larsen KE, Schmitz Y, Troyer MD, Mosharov E, Dietrich P, Quazi AZ, Savalle M, Nemani V, Chaudhry FA, Edwards RH, Stefanis L, Sulzer D: α-Synuclein overexpression in PC12 and chromaffin cells impairs catecholamine release by interfering with a late step in exocytosis. J Neurosci 2006, 26:11915–11922

Human Molecular Genetics, 2009, Vol. 18, No. 4 *723–736*
doi:10.1093/hmg/ddn403
Advance Access published on November 27, 2008

Severe neurological phenotypes of Q129 DRPLA transgenic mice serendipitously created by *en masse* expansion of CAG repeats in Q76 DRPLA mice

Toshiya Sato[1], Masami Miura[5], Mitsunori Yamada[2], Takayuki Yoshida[6,†], Jonathan D. Wood[7,‡], Ikuru Yazawa[10], Masao Masuda[5], Takeo Suzuki[5,11], Ryong-Moon Shin[5,¶], Hau-Jie Yau[12], Fu-Chin Liu[12], Takayoshi Shimohata[3], Osamu Onodera[4], Christopher A. Ross[7,8,9], Motoya Katsuki[13], Hitoshi Takahashi[2], Masanobu Kano[6,§], Toshihiko Aosaki[5] and Shoji Tsuji[14,*]

[1]Department of Comparative and Experimental Medicine, [2]Department of Pathology, [3]Department of Neurology and [4]Department of Molecular Neuroscience, Brain Research Institute, Niigata University, Niigata 951-8585, Japan, [5]Neural Circuits Dynamics Research Group, Tokyo Metropolitan Institute of Gerontology, Itabashi-ku, Tokyo 173-0015, Japan, [6]Department of Cellular Neurophysiology, Graduate School of Medical Science, Kanazawa University, Kanazawa, Ishikawa 920-8640, Japan, [7]Department of Psychiatry, [8]Department of Neurology and [9]Department of Neuroscience, The Johns Hopkins University School of Medicine, Baltimore, MD 21287, USA, [10]Laboratory of Research Resources, National Institute for Longevity Sciences, Obu, Aichi 474-8522, Japan, [11]Department of Anesthesiology, School of Medicine, Juntendo University, Bunkyo-ku, Tokyo 113-8421, Japan, [12]Institute of Neuroscience, National Yang-Ming University, Li-Rum Street, Taiwan 11221, Taiwan, [13]National Institute for Basic Biology, Okazaki National Research Institutes, Okazaki, Aichi 444-8585, Japan and [14]Department of Neurology, Graduate School of Medicine, University of Tokyo, Bunkyo-ku, Tokyo 113-8655, Japan

Received August 1, 2008; Revised and Accepted November 25, 2008

We herein provide a thorough description of new transgenic mouse models for dentatorubral–pallidoluysian atrophy (DRPLA) harboring a single copy of the full-length human mutant *DRPLA* gene with 76 and 129 CAG repeats. The Q129 mouse line was unexpectedly obtained by *en masse* expansion based on the somatic instability of 76 CAG repeats *in vivo*. The mRNA expression levels of both Q76 and Q129 transgenes were each 80% of that of the endogenous mouse gene, whereas only the Q129 mice exhibited devastating progressive neurological phenotypes similar to those of juvenile-onset DRPLA patients. Electrophysiological studies of the Q129 mice demonstrated age-dependent and region-specific presynaptic dysfunction in the globus pallidus and cerebellum. Progressive shrinkage of distal dendrites of Purkinje cells and decreased currents through α-amino-3-hydroxy-5-methyl-4-isoxazolepropionic acid and γ-aminobutyrate type A receptors in CA1 neurons were also observed. Neuropathological studies of the Q129 mice revealed progressive brain atrophy, but no obvious neuronal loss, associated with massive neuronal intranuclear accumulation (NIA) of mutant proteins with expanded polyglutamine stretches starting on postnatal day 4, whereas NIA in the Q76 mice appeared later with regional specificity to the vulnerable regions of DRPLA. Expression profile analyses demonstrated age-dependent down-regulation of genes, including those relevant to synaptic

*To whom correspondence should be addressed. Tel: +81 358006542; Fax: +81 358006844; Email: tsuji@m.u-tokyo.ac.jp
†Present address: Department of Neuropharmacology, Graduate School of Medicine, Hokkaido University, Kita-ku, Sapporo 060-8638, Japan.
‡Present address: Academic Neurology Unit, The University of Sheffield Medical School, Beech Hill Road, Sheffield S10 2RX, UK.
¶Present address: Department of Psychiatry, McLean Hospital, Harvard Medical School, Belmont, MA 02478, USA.
§Present address: Department of Neurophysiology, Graduate School of Medicine, University of Tokyo, Bunkyo-ku, Tokyo 113-0033, Japan.

functions and CREB-dependent genes. These results suggest that neuronal dysfunction without neuronal death is the essential pathophysiologic process and that the age-dependent NIA is associated with nuclear dysfunction including transcriptional dysregulations. Thus, our Q129 mice should be highly valuable for investigating the mechanisms of disease pathogenesis and therapeutic interventions.

INTRODUCTION

Dentatorubral–pallidoluysian atrophy (DRPLA; MIM 125370) is a devastating, autosomal-dominant neurodegenerative disease characterized by progressive dementia, cerebellar ataxia, choreoathetosis, myoclonus and epilepsy in various combinations depending on the age at onset (1). As indicated by the name, autopsied brains show a selective neuronal loss associated with astrocytosis in the dentatorubral and pallidoluysian (DRPL) systems (2). In 1994, we and another group, focusing on genes containing CAG repeats (3), found that DRPLA is caused by an unstable expansion of CAG repeats coding for polyglutamine (polyQ) stretches in exon 5 of the *DRPLA* gene on chromosome 12p13.31 (4,5). To date, polyQ expansions have been identified as the pathogenic mutations in nine neurodegenerative diseases including Huntington's disease (HD), spinal and bulbar muscular atrophy, DRPLA and various forms of dominant spinocerebellar ataxias (SCAs) (6).

The discovery of neuronal intranuclear inclusions (NIIs) not only in brains of transgenic mice (7) but also in autopsied brains with polyQ diseases (8,9) provided new insight into neuronal nuclei as a potentially important site of pathogenic mechanisms. More importantly, we demonstrated that a diffuse accumulation of a mutant DRPLA protein (atrophin-1) in the neuronal nuclei of autopsied brains, rather than the formation of NIIs, is the predominant pathologic condition involving a wide range of central nervous system (CNS) regions far beyond the vulnerable DRPL systems (10). To further emphasize the involvement of nuclear dysfunction in polyQ diseases, we have demonstrated that expanded polyQ stretches bind to TATA-binding protein (TBP)-associated factors ($TAF_{II}130$) and cAMP response element-binding protein (CREB)-binding protein (CBP), which are components of transcriptional regulators (11,12). Taken together, these findings strongly suggest that essential pathogenetic processes occur in neuronal nuclei. The molecular mechanisms of neurodegeneration, however, remain to be elucidated.

To investigate these molecular mechanisms, studies on animal models precisely replicating all the processes in the human brain would be indispensable. For high-quality animal models, the expression of a full-length mutant gene under the control of its own promoter is preferable to those expressing truncated mutant proteins or under the control of potent heterologous promoters. To meet these requirements, we have generated transgenic mice harboring a single copy of the full-length human mutant *DRPLA* gene containing 76 CAG repeats (13). These Q76 mice did not exhibit obvious neurological phenotypes. During intensive breeding of Q76 mice, however, we unexpectedly found a mosaic mouse harboring largely expanded CAG repeats (Q129), in addition to the 76 repeats from progenitor mice, which bred transgenic offspring carrying 129 CAG repeats exhibiting distinct behavioral abnormalities. The Q129 mice showed severe neurological phenotypes with progressive brain atrophy and premature death. Some neuropathological findings of the Q129 mice at 14 weeks of age focusing on morphometric analysis have recently been reported, which demonstrate atrophy of the perikarya and dendrites, and a decrease in the number and size of the spines without any obvious neuronal loss (14). We herein report a thorough characterization of the phenotypes of Q129 mice, including electrophysiological abnormalities, neuropathological findings focusing on age-dependent neuronal intranuclear accumulation (NIA) of mutant DRPLA proteins and nuclear dysfunction assessed by expression profiling. As shown here, Q129 mice harboring a single copy of the full-length *DRPLA* gene have many advantages over the previous Q76 mice, and should serve as excellent models for exploring the molecular mechanisms of CAG repeat instability, disease pathogenesis and, furthermore, therapeutic intervention for polyQ diseases.

RESULTS

En masse expansion of CAG repeats occurred via somatic instability in a Q76 mouse

We previously established three transgenic lines, which were generated by the transfer of a cosmid genomic clone containing the full-length human mutant *DRPLA* gene with 78 CAG repeats (13). Although the mice showed intergenerational instabilities of CAG repeats similar to those observed in DRPLA patients, no obvious abnormal phenotypes were detected. To investigate intergenerational instabilities, we continued our extensive breeding of the Drm21 line carrying the 76 CAG repeats (Q76 mice). During the process, we unexpectedly noticed one male mouse (EF121) carrying both 76 and 129 CAG repeats among over 2000 hemizygous mice [Fig. 1A, Mosaic (Q129-76)]. After the birth of the EF121 mouse, the male parent of the EF121 mouse bred only Q76 or non-transgenic (non-TG) mice ($n = 66$ and 54, respectively). On the other hand, the highly expanded 129 CAG repeats, of which sequence was uninterrupted (unpublished data), were transmitted from the EF121 mouse to certain offspring exhibiting behavioral abnormalities (Q129 mice). These results suggest that the EF121 mouse is a mosaic with respect to the length of CAG repeats of the transgene and that the 129 CAG repeats were presumably generated by the *en masse* expansion of the 76 CAG repeats at the early embryonic stage.

Although the EF121 mosaic mouse was smaller than the Q76 mice and exhibited a slightly ataxic phenotype with age, the mouse was able to continue to breed and sired 528 mice by 122 weeks of age. The percentages of transgenic offspring of Q129, Q76 and non-TG mice bred from the EF121 mosaic mouse were 19% ($n = 98$), 32% ($n = 170$) and 49% ($n = 260$), respectively. Because one-half of the offspring were non-TG mice, the EF121 mosaic mouse was considered to be a hemizygote. Furthermore, the segregation ratios of 19

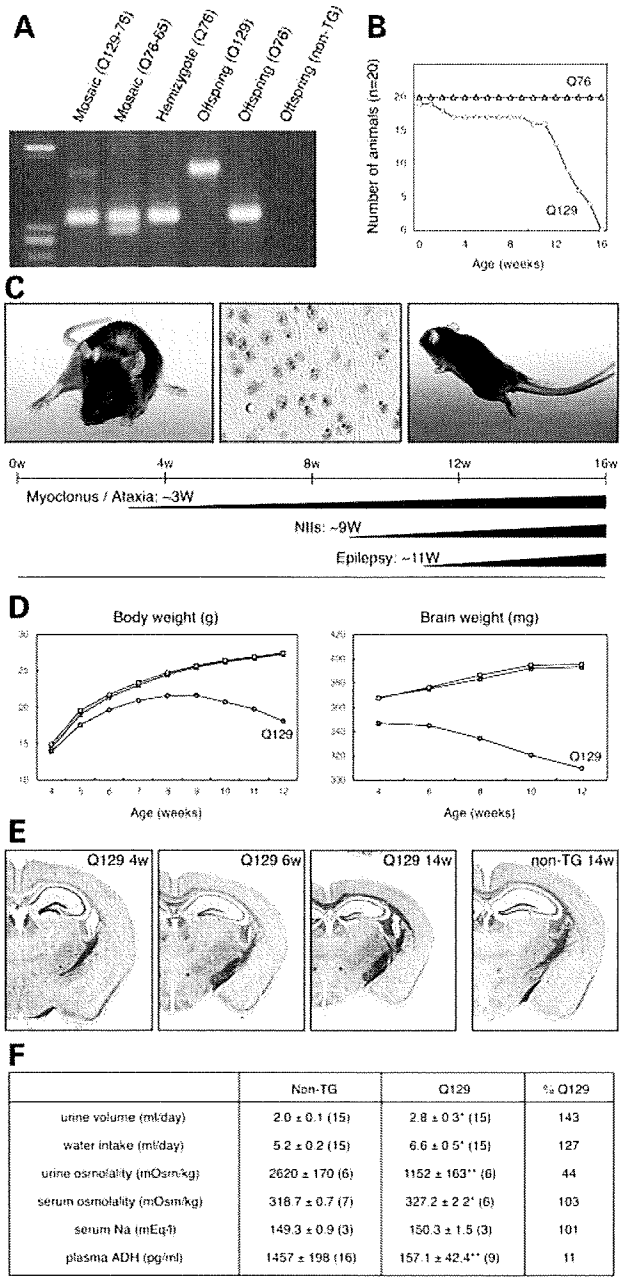

	Non-TG	Q129	% Q129
urine volume (ml/day)	2.0 ± 0.1 (15)	2.8 ± 0.3* (15)	143
water intake (ml/day)	5.2 ± 0.2 (15)	6.6 ± 0.5* (15)	127
urine osmolality (mOsm/kg)	2620 ± 170 (6)	1152 ± 163** (6)	44
serum osmolality (mOsm/kg)	318.7 ± 0.7 (7)	327.2 ± 2.2* (6)	103
serum Na (mEq/l)	149.3 ± 0.9 (3)	150.3 ± 1.5 (3)	101
plasma ADH (pg/ml)	1457 ± 198 (16)	157.1 ± 42.4** (9)	11

Figure 1. Generation of Q129 transgenic mice and disease phenotypes. (**A**) PCR analysis of tail DNA revealed two hemizygous mosaic mice (Q129-76 and Q76-65), a hemizygous mouse (Q76) and the offspring of the Q129-76 mosaic mouse showing three genotypes (Q129, Q76 and non-TG). The lane for the Q129-76 mosaic mouse showed a faint extra band of a much larger size than the band corresponding to 76 CAG repeats. The large changes in the size of CAG repeats resulted in not only expansion (Q129-76), but also contraction (Q76-65). (**B**) Kaplan–Meier survival curves of Q76 (triangles) and Q129 (circles) mice, showing premature death of Q129 mice ($n = 20$). (**C**) Representative photographs of the Q129 mice at 12 weeks (W), showing ataxic phenotype (left panel), ubiquitinated NIIs (middle panel) and epileptic seizure (right panel). (**D**) Changes in body and brain weights of the Q129 (circles), Q76 (triangles) and non-TG (rectangles) mice. Each value and number of replicates is shown in Supplementary Material, Tables S1 and S2. (**E**) Cross-sections of brains of the Q129 mice (4W, 6W and 14W) and non-TG littermate (14W) (Klüver–Barrera staining), showing progressive reduction in brain size of Q129 mice. (**F**) Results of laboratory tests indicate central diabetes insipidus. Each value indicates mean ± S.E.M. Unpaired *t*-test, $^*P < 0.05$, $^{**}P < 0.01$. Numbers of replicates are shown in parentheses.

and 32% suggested that the *en masse* expansion of the CAG repeats had occurred either at the two-cell or four-cell stage. The Q129 mice were established by *in vitro* fertilization because of their decreased fertility. The fertilizing ability of spermatozoa from the Q129 mice was comparable to that of the wild-type mice, suggesting that the reduced fertility is due to behavioral abnormalities.

Phenotypes of Q129 mice are similar to those of juvenile-onset DRPLA patients

The onset of symptoms was as early as 3 weeks of age, at which the Q129 mice began to show myoclonic movements and mild ataxia (Fig. 1C). When held by the tail, the myoclonic movements were more evident with limbs outstretched. The clasping of hindlimbs was hardly observed. The myoclonic movements and ataxia rapidly progressed, and epilepsy was observed at around 11 weeks. Initially, epilepsy was induced by tactile stimuli and at the later stage, it occurred spontaneously, even in their home cages. The rapid progression of the disease phenotype was followed by premature death, and all the Q129 mice died by 16 weeks (Fig. 1B and C; Supplementary Material, Videos S1 and S2, ataxia and epilepsy, respectively). The severe neurological phenotypes observed in the Q129 mice, namely myoclonus and epilepsy, were quite similar to those observed in juvenile-onset DRPLA patients with onset before the age of 20 (1,15). These phenotypes are in striking contrast to those of the Q76 mice that do not show any obvious neurological phenotypes.

The brain weight was less than that of the Q76 or non-TG mice at 4 weeks of age, even at a time when body weight did not change. Along with the disease progression, the brain weight of the Q129 mice further decreased after 6 weeks of age prior to the decrease in body weight (Fig. 1D; Supplementary Material, Tables S1 and S2). The examination of brain cross-sections further demonstrated the age-dependent decrease in the brain size of the Q129 mice at 4, 6 and 14 weeks of age (Fig. 1E). In addition, the Q129 mice became polyuric around 5 weeks of age, a phenomenon that was not observed in the Q76 mice. Detailed analyses of water balance were conducted at 8 weeks of age. The Q129 mice showed increased urine volume, water intake and serum osmolality, and reduced urine osmolality (Fig. 1F). Furthermore, we found a drastic reduction in the plasma vasopressin (anti-diuretic hormone) level, confirming that the Q129 mice suffered from central diabetes insipidus.

Dysfunction of pallidal and cerebellar neurons correlates with disease manifestations and progression

We first conducted electrophysiological studies of the globus pallidus (GP) and cerebellum, because these structures are highly associated with neuropathological changes in DRPLA. Using the Q129 and non-TG mice at 4–5 weeks of age, we performed whole-cell recordings from pallidal neurons. Excitatory (EPSCs) and inhibitory postsynaptic currents (IPSCs) were evoked by activating the sub-thalamopallidal and striatopallidal pathways, respectively. We did not detect any significant differences in input–output (I–O) relationships (Fig. 2Aa). In addition, current–voltage (I–V) relationships and the

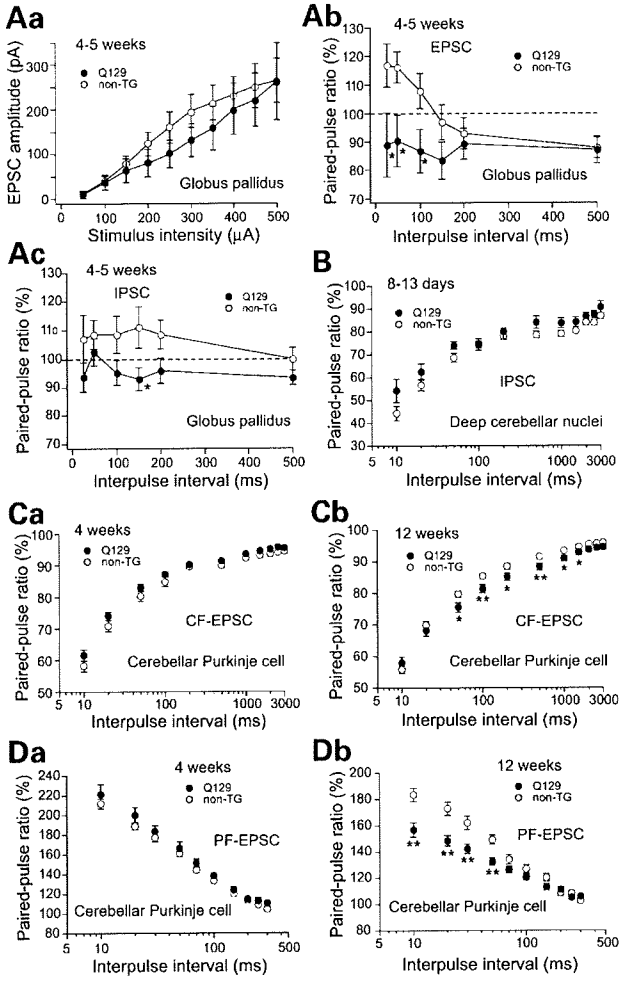

Figure 2. Age-dependent abnormalities of synaptic transmission in GP and cerebellum. Pallidal and cerebellar slices were obtained from the Q129 mice (filled circles) and non-TG mice (open circles) at various ages as indicated in each figure. (**Aa**–**Ac**) Whole-cell recordings from pallidal neurons of the Q129 and non-TG mice at 4–5 weeks of age. I–O relationship for EPSC (**Aa**), PPRs for EPSC (**Ab**) and IPSC (**Ac**) in GP. EPSCs and IPSCs were evoked by stimulating the sub-thalamopallidal and striatopallidal pathways, respectively, at 0.1 Hz with a bipolar tungsten electrode (100–500 μs, 100–800 μA). IPSCs were recorded at a holding potential of −10 mV in the presence of CNQX and D-AP5. EPSCs of the Q129 mice ($n = 14$) tended to be smaller than those of the non-TG mice ($n = 21$), which showed no statistically significant difference (**Aa**). PPRs for EPSC (**Ab**) and IPSC (**Ac**) in the Q129 mice ($n = 12$ and 11, respectively) decreased as compared with those of the non-TG mice ($n = 22$ and 15, respectively), resulting in the conversion of PPF to PPD in the Q129 mice at 4–5 weeks of age. (**B**) PPR for IPSC in FN on postnatal days 8–13. IPSCs were evoked by stimulating bundles of putative PC axons. There was no significant difference between the Q129 mice ($n = 12$) and the non-TG mice ($n = 30$). (**Ca**–**Db**) Age-dependent changes in PPRs for CF-EPSCs and PF-EPSCs. CF-EPSCs were recorded from PCs at 4 (**Ca**) and 12 weeks (**Cb**) of age in the Q129 ($n = 19$ and 27, respectively) and non-TG mice ($n = 20$ and 30, respectively). PF-EPSCs were recorded from PCs at 4 (**Da**) and 12 weeks (**Db**) of age in the Q129 ($n = 14$ and 27, respectively) and non-TG mice ($n = 22$ and 28, respectively). For focal stimulation in the cerebellar slices, we used a bipolar tungsten electrode (for PC axons) and glass pipettes (5–10-μm tip diameter) filled with standard saline (for CFs and PFs), and applied square pulses (duration, 100 μs; amplitude, 0–90 V) at 0.5 Hz. Bundles of putative PC axons were stimulated in the white matter 100–200 μm away from the FN. CFs were stimulated in the granule cell layer 50–100 μm away from the PC soma. PFs were stimulated in the middle of the molecular layer. Each value indicates mean ± S.E.M. Unpaired *t*-test, $^{*}P < 0.05$, $^{**}P < 0.01$. Note that the abscissas of **B**–**Db** are shown in the logarithmic scale.

amplitudes of both *N*-methyl-D-aspartate (NMDA) and α-amino-3-hydroxy-5-methyl-4-isoxazolepropionic acid (AMPA) components of EPSCs were not significantly different (unpublished data). In contrast, the paired pulse facilitation (PPF) of EPSCs and IPSCs was clearly converted to paired pulse depression (PPD) in the Q129 mice (Fig. 2Ab and Ac), suggesting presynaptic dysfunction in GP of the Q129 mice at 4–5 weeks of age.

For electrophysiological studies of the cerebellum, we conducted whole-cell recordings from medium to large neurons in the fastigial nucleus (FN) obtained from young asymptomatic mice aged 8–13 days. IPSCs evoked by stimulating putative Purkinje cell (PC) axons displayed PPD in both non-TG and Q129 mice (Fig. 2B). There was no significant difference in the extent of PPD. Thus, on postnatal days 8–13 before the manifestation of ataxia, transmission from PCs to neurons in FN (one of the deep cerebellar nuclei) in the Q129 mice was apparently normal. Further studies of neurons in the GP and FN at later stages could not be performed because of the limited time window suitable for such electrophysiological analyses.

To investigate age-dependent changes in the cerebellum, we next compared the electrophysiological properties of PCs at 4 and 12 weeks of age. The passive membrane properties of PCs were calculated by recording membrane currents in response to hyperpolarizing voltage steps, as described previously (16). We found that the C2 of the Q129 mice, representing the lumped membrane capacitance of the PC's dendritic tree, was significantly smaller than that of the non-TG mice at 12 weeks of age ($P < 0.01$), whereas no significant changes were observed at 4 weeks of age (Table 1). In addition, R3 of the Q129 mice, representing the lumped resistance of the PC's dendritic tree, tended to be greater than that of the non-TG mice at 12 weeks of age. These results suggest that the PC's dendritic trees of the Q129 mice markedly shrank in a time-dependent manner.

We then examined whether excitatory synaptic transmission to PCs is altered in the Q129 mice. We recorded EPSCs from PCs by stimulating climbing fibers (CFs: axons of inferior olivary neurons) or parallel fibers (PFs: axons of granule cells). We first confirmed that the number of CFs innervating a PC was not significantly different between the non-TG and Q129 mice at 4 or 12 weeks of age (unpublished data). As for the kinetics of CF-EPSCs, the rise time or amplitude was not significantly altered in the Q129 mice except for a slight decrease in the decay time constant in the Q129 mice at 4 and 12 weeks of age (Table 1). At 4 weeks of age, there was no significant difference in the extent of PPD of CF-EPSC or PPF of PF-EPSC (Fig. 2Ca and Da). At 12 weeks of age, however, paired pulse ratios (PPRs) for CF-EPSC and PF-EPSC in the Q129 mice were significantly smaller than those in the non-TG mice at interpulse intervals of 50–1500 ms and those at intervals of shorter than 50 ms, respectively (Fig. 2Cb and Db).

Dysfunction of synaptic transmission in hippocampal CA1 pyramidal cells

Although the hippocampus is not a severely affected region in DRPLA, NIA of mutant DRPLA proteins was observed in juvenile-onset DRPLA patients (10), and also confirmed in

Table 1. Electrophysiological parameters of PCs

	Non-TG	Q129
Postnatal 4 weeks		
Passive membrane properties[a]	$n = 6$	$n = 11$
C1 (pF)	60.4 ± 8.8	69.8 ± 10.0
C2 (pF)	617.3 ± 58.8	571.2 ± 46.8
R1 (MΩ)	14.8 ± 3.4	13.2 ± 1.2
R2 (MΩ)	21.3 ± 5.1	19.4 ± 2.0
R3 (MΩ)	308.1 ± 68.2	211.0 ± 29.9
CF-EPSC	$n = 15$	$n = 18$
10–90% rise time (ms)	0.4 ± 0.01	0.4 ± 0.01
Decay time constant (ms)[b]	7.7 ± 0.3**	6.6 ± 0.3**
Amplitude at −10 mV (pA)	1114.1 ± 111.4	1126.2 ± 139.9
Amplitude at +50 mV (pA)	768.1 ± 179.6	812.2 ± 241.8
Postnatal 12 weeks		
Passive membrane properties[a]	$n = 14$	$n = 19$
C1 (pF)	95.5 ± 13.4	80.8 ± 11.1
C2 (pF)	629.9 ± 63.5**	332.6 ± 18.9**
R1 (MΩ)	11.1 ± 0.6	11.4 ± 1.1
R2 (MΩ)	15.8 ± 3.8	16.7 ± 1.7
R3 (MΩ)	241.2 ± 47.4	405.3 ± 76.5
CF-EPSC	n=23	$n = 26$
10–90% rise time (ms)	0.4 ± 0.03	0.4 ± 0.01
Decay time constant (ms)[b]	6.9 ± 0.3**	5.9 ± 0.3**
Amplitude at −10 mV (pA)	1150.9 ± 98.8	1312.0 ± 140.4
Amplitude at +50 mV (pA)	1085.2 ± 182.9	1771.3 ± 297.7

[a] Parameters for passive membrane properties are calculated according to the model described by Llano *et al.* (16), which distinguishes two regions of PCs: region 1, representing the soma and the main proximal dendrites, and region 2, representing the dendritic tree. C1 and C2 represent the lumped membrane capacitance of regions 1 and 2, respectively. R1 represents the pipette access resistance. Region 2 is linked to region 1 by resistor R2, representing the lumped resistance between the main proximal dendrite and each membrane region of distal dendrites. R3 represents the lumped resistance of the dendritic tree of PCs. C1, C2, R1 and R2 are calculated from the initial capacitive currents in response to hyperpolarizing voltage steps (500-ms duration) from −70 to −80 mV. R3 is measured from the steady-state currents in response to hyperpolarizing voltage steps (500-ms duration) from −80 to −85 mV.
[b] Decay time constants for CF-EPSC are measured by fitting EPSC decay with a single exponential. The holding potential was −80 mV.
All data are expressed as mean ± S.E.M.
**$P < 0.01$ (t-test).

Q76 (Table 2) and Q129 mice (14), indicating that the hippocampus may well be involved in the pathological processes of DRPLA. To evaluate the electrophysiological properties of hippocampal CA1 pyramidal cells, we first analyzed basal synaptic transmission by applying electrical stimuli of increasing intensity to the Schaffer collateral/commissural pathway using Q129 and non-TG mice at 12–15 weeks of age. The extracellular recordings showed that the field excitatory postsynaptic potential (fEPSP) slopes of the Q129 mice were significantly smaller than those of the non-TG mice at 12–15 weeks of age (Fig. 3A). A significantly enhanced PPF was also observed in the Q129 mice (Fig. 3B at 100 ms, $P = 0.024$; at 150 ms, $P = 0.002$), suggesting presynaptic dysfunction.

In the whole-cell recordings from CA1 neurons, the ratio of NMDA/AMPA currents in the Q129 mice was significantly larger than that in the non-TG mice, despite the observation that I–V relationships of AMPA, NMDA and γ-aminobutyrate type A ($GABA_A$) currents were unchanged (unpublished data). To further investigate the mechanisms underlying the increased ratio of NMDA/AMPA currents, we compared responses to the agonists of AMPA, NMDA and $GABA_A$ receptors. AMPA-induced inward currents were significantly smaller in the Q129 mice than in the non-TG mice across the five concentrations tested (Fig. 3Ea), whereas there were no significant changes in NMDA-induced inward currents (Fig. 3Eb). Similar to AMPA currents, $GABA_A$-induced outward currents were significantly smaller in the Q129 mice than in the non-TG mice at elevated muscimol concentrations (Fig. 3Ec).

We next analyzed the long-term potentiation (LTP) of fEPSPs in the hippocampal CA1 region. LTP induced by one train of tetanic stimulation lasted for more than 4 h in the non-TG mice, whereas it subsided within 2 h in the Q129 mice (Fig. 3C). The average fEPSP slope within a time window of 120–180 min after tetanus in the Q129 mice was 98.7 ± 9.3%, which was significantly lower than that in the non-TG mice (132.8 ± 4.5%, $P = 0.004$). In contrast, four trains of tetanic stimulation induced late-phase LTP in both genotypes to the same extent (Fig. 3D).

Age- and expanded-polyQ-length-dependent NIA of mutant DRPLA proteins

In accordance with our previous findings in the Q129 mice at 14 weeks of age (14), an age-dependent decrease in the brain size of the Q129 mice was evident (Fig. 1E), but neuronal loss or astrocytosis was not evident despite the progressive brain atrophy (Fig. 4). In hematoxylin- and eosin-stained preparations, small eosinophilic intranuclear inclusions were detectable in some neurons of restricted CNS regions of the Q129 mice after 12 weeks of age (unpublished data). In immunohistochemical analysis using anti-ubiquitin antibodies, they were easily detected after 9 weeks of age as ubiquitinated NIIs in multiple CNS regions such as the cerebral cortex, GP, subthalamic nucleus (luysian body), brainstem tegmentum and deep cerebellar nuclei (Fig. 1C). It should be noted, however, that NIIs were formed much later than the onset of neurological phenotypes, suggesting that the disease phenotypes do not arise from the formation of NIIs. In contrast to the Q129 mice, we did not detect any evidence of NIIs in the brain of Q76 mice even at 122 weeks of age (unpublished data).

To find age-dependent changes focusing on the regional distribution of NIA, we performed immunohistochemical analyses of the Q76 and Q129 mice at various weeks of age using highly diluted 1C2 (1:16 000). At this dilution, no background immunoreactivities were detected in the brain of the non-TG mice, confirming that 1C2 immunoreactivity is specific to the expanded polyQ stretches of mutant proteins (Fig. 4A, right panels) (10). In contrast to the non-TG mice, 1C2 immunoreactivity was clearly evident as a diffuse nuclear labeling of neurons in the 4-week-old brain of the Q129 mice (Fig. 4A, middle panels). The nuclear labeling, namely NIA, was strong and extended to most of the CNS regions including the brainstem, spinal cord and the regions evaluated for the above-mentioned electrophysiological properties. It should be noted that NIA, which was observed at 4 weeks of age in the Q129 mice, occurred much earlier than the appearance of NIIs after approximately 9 weeks of age. To determine when NIA becomes apparent, we further

Table 2. Distribution of NIA of expanded polyQ stretches in Q76 mice

Region	Gestational age 4W	8W	14W	Region	Gestational age 4W	8W	14W
Cerebral cortex				Thalamic nuclei			
II	−	+	++	Centrolateral	−	−	++
III	−	+	+++	Ventroposterior	−	−	+
IV	+	+++	+++	Reticular	−	−	++
V	−	+	+	Subthalamic nucleus	+	++	+++
VI	−	++	+++	Hypothalamic nuclei	−	+	++
Piriform cortex	−	+	++	Substantia nigra			
Caudate-putamen	−	+	++	Pars compacta	−	++	+++
Globus pallidus	+	++	+++	Pars reticulata	−	+	++
Hippocampus				Superior colliculus	−	+	+++
CA1	−	−	+	Periaqueductal gray	−	+	++
CA2	−	−	+	Deep mesencephalic nucleus	−	+	+++
CA3	−	−	+	Red nucleus	+	++	+++
Dentate gyrus				Pontine nuclei	−	+	+++
Granule cell layer	−	−	+	Pontine reticular nucleus	+	++	+++
Polymorphic cell layer	−	−	+	Vestibular nucleus	−	++	+++
Amygdaloid nuclei	+	+	++	Facial nucleus	−	−	−
Lateral habenular nucleus	−	+	+++	Inferior olive	−	−	−
Medial habenular nucleus	−	−	−	Gigantocellular reticular field	+	++	+++
Thalamic nuclei				Purkinje cell	−	−	−
Mediodorsal	−	−	+	Granule cell	−	+	++
Centromedial	−	−	++	Cerebellar nuclei	+	++	+++

At 4 weeks of age, nuclear labeling was detected not only in the DRPL systems, but also in some brain regions including the cerebral cortex and brainstem nuclei. Thereafter, the number and intensity of labeled neurons increased gradually throughout the brain with a specific distribution pattern. Percentage of labeled neurons: −, none; +, <30%; ++, 30–70%; +++, >70%.

analyzed the Q129 mice on embryonic and postnatal days. NIA was not observed in the brain of Q129 mice on postnatal day 1 (P1), but became detectable on P4, confirming age-dependent NIA of mutant DRPLA proteins (Fig. 4B).

Interestingly, NIA was also observed in the Q76 mouse brain despite the Q76 mice not showing any obvious neurological phenotypes. In contrast to the Q129 mice, the intensity of NIA was weak in the brains of Q76 mice, but increased with age (Fig. 4A, left panels). The regional distribution of NIA in the Q76 mice was analyzed semiquantitatively (Table 2). NIA was first detectable at 4 weeks of age in limited CNS regions, such as the cerebellar nuclei, red nucleus, GP, subthalamic nucleus and a few other regions including the cerebral cortex of the Q76 mice. It is noteworthy that the former four regions are the sites known to be the most vulnerable to DRPLA (1,2). Furthermore, the distribution of NIA in the brains of Q76 mice at 14 weeks of age became similar to that of NIIs in the brains of Q129 mice.

Since 1C2 immunoreactivity varies depending on the length of polyQ stretches, immunohistochemical analyses with 1C2 may produce some bias in terms of accumulation of mutant DRPLA proteins with different lengths of expanded polyQ stretches. We further conducted immunohistochemical analyses using APG840 raised against residues 425–439 of the DRPLA protein (10) that correspond to the upstream region of the polyQ stretches. In contrast to 1C2, APG840 recognized not only human mutant DRPLA proteins, but also endogenous mouse wild-type DRPLA proteins (Fig. 4C). Although background nuclear staining was observed in the non-TG mice as APG840 recognized mouse DRPLA protein, strong nuclear staining was observed in the Q129 mice at as early as 4 weeks of age. In the Q76 mice, mild but increased staining was observed at 14 weeks compared with that at 4 weeks. These findings further confirm polyQ-length-dependent and age-dependent intranuclear accumulation of mutant DRPLA proteins.

Massive accumulation of mutant DRPLA proteins in Q129 mouse brain

First, we performed quantitative analyses of the mRNA expression levels of the human *DRPLA* transgene and endogenous mouse *DRPLA* gene in the brains of the Q76 and Q129 mice at 8 weeks of age by competitive reverse transcription–polymerase chain reaction (RT–PCR) (Fig. 5A). After confirming the validity of the quantitative analysis by PCR, the mRNA expression levels of the transgenes of the Q129 and Q76 mice were determined to be ~80% of the mouse endogenous level.

Western blot analysis was performed using three antibodies: C580 (17; a polyclonal antibody against the carboxyl terminus of the DRPLA protein), AP142 (18; a polyclonal antibody against residues 425–439) and 1C2 (specifically recognizes expanded polyQ stretches). In the total homogenates of the mouse brain, two bands corresponding to the full-length mouse endogenous DRPLA protein (200 kDa) and transgene-derived DRPLA proteins (210 and 220 kDa in Q76 and Q129, respectively) were detected using C580, whereas only the lower band corresponding to the full-length mouse DRPLA protein was observed for the non-TG mice (Fig. 5B). In addition to the 200-kDa band, a 100-kDa band was detected in human autopsied control brain, consistent with previous observations on human DRPLA brains employing C580 (17). The intensities of the bands of the full-length DRPLA proteins of Q129 were much weaker than those corresponding

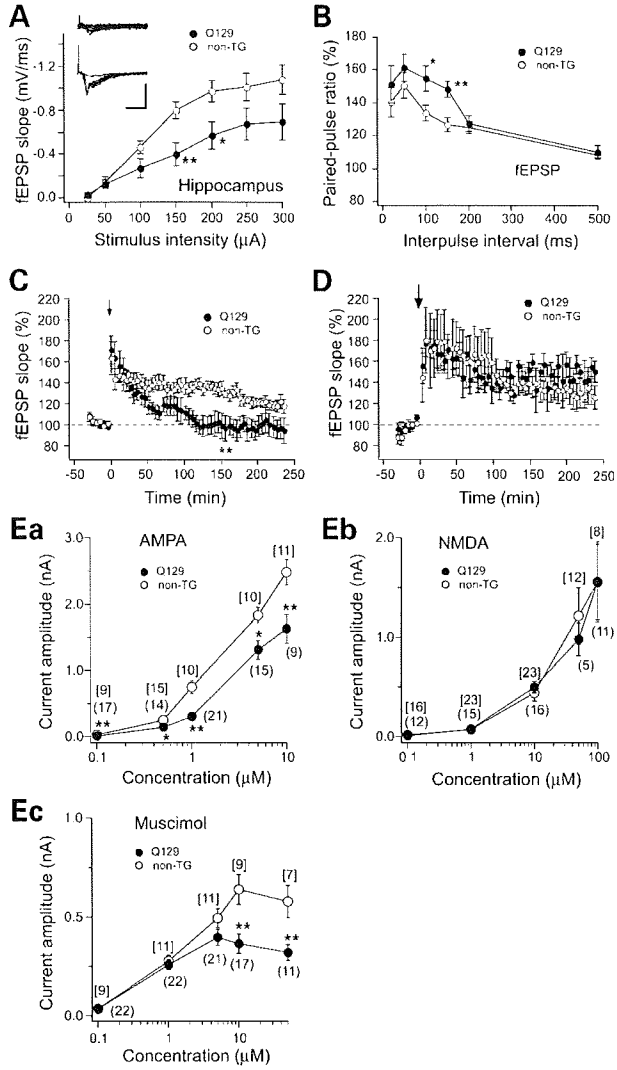

Figure 3. Abnormalities of synaptic transmission and plasticity in hippocampus. Hippocampal slices were obtained from the Q129 mice (filled circles) and the non-TG mice (open circles) at 12–15 weeks of age. (**A**) The I–O relationship showed a significant attenuation of the responsiveness of CA1 pyramidal cells in the Q129 mice ($n = 12$) as compared with that in the non-TG mice ($n = 13$). The slopes of fEPSPs evoked by stimulating the Schaffer collateral/commissural pathway are plotted against stimulus intensity. Inset: examples of fEPSPs of the Q129 (upper) mouse and the non-TG (lower) mouse. Scale bars: 2 mV/10 ms. (**B**) The PPR for the fEPSP slope of CA1 hippocampal cells in the Q129 mice ($n = 12$) was enhanced as compared with that in the non-TG mice ($n = 13$) at 13–15 weeks of age. (**C**) LTP induced by one train of tetanus (a small arrow) subsided within 120 min in the Q129 mice ($n = 10$), whereas LTP in the non-TG mice ($n = 10$) lasted much longer. (**D**) Late-phase LTP induced by four trains of tetanus (a large arrow) was not significantly different between the Q129 mice ($n = 5$) and the non-TG mice ($n = 5$). Data in **C** and **D** are normalized for each slice with respect to the average slope recorded during the baseline. (**Ea**–**Ec**) Pharmacological evidence for functional down-regulation of AMPA and $GABA_A$ receptors in hippocampus of Q129 mice at 12–15 weeks of age. AMPA-induced inward current (**Ea**) was recorded at a holding potential of −60 mV in the presence of 0.1 mM cyclothiazide, which prevents the rapid desensitization of AMPA receptors and 0.5 μM TTX. NMDA-induced inward current (**Eb**) was recorded at a holding potential of −40 mV in the presence of 20 μM glycine and 0.5 μM TTX in Mg^{2+}-free ACSF. Muscimol-induced outward current (**Ec**) was recorded at a holding potential of 0 mV. Drug exposure time was 1 min throughout the experiments. The flow rate was 2–3 ml/min. Each value indicates mean ± S.E.M. Unpaired *t*-test, $^*P < 0.05$, $^{**}P < 0.01$.

to the mouse endogenous DRPLA proteins or those of Q76, which may reflect the highly aggregatable nature of mutant DRPLA proteins with highly expanded polyQ stretches that may be resistant to extraction or solubilization procedures. Although the reason why the intensities of full-length mutant proteins decreased in the Q129 mice was unclear, a similar observation was described for $SCA1^{154Q/2Q}$ mice (19). The intensities of the bands detected by C580 were similar throughout the time course of 4, 8 and 12 weeks of age.

To further analyze the proteins accumulating in the nucleus, we prepared nuclear fractions employing the sucrose gradient centrifugation procedure as previously described (20) from the brains of Q129, Q76 and non-TG littermates at 12 weeks of age, and performed western blot analysis using AP142 that recognizes the segment upstream of polyQ stretches. A massive amount of smear migrating between the stacking gel and the band corresponding to the full-length mutant protein was observed for the Q129 mice, in addition to human full-length and truncated bands as well as the mouse endogenous band (Fig. 5C). The truncated proteins were also recognized by 1C2 (unpublished data) and thus specific for mutant DRPLA proteins as described previously (20). The smear was far more intense for the Q129 mice than for the Q76 mice, confirming the polyQ-length-dependent nuclear accumulation of the mutant proteins with expanded polyQ stretches. The smearing pattern was also observed in AT-FL-65Q-150 mice (Fig. 5C; lane 1) as previously described. AT-FL-65Q-150 mice are transgenic mice carrying full-length DRPLA cDNA under the control of the prion promoter and expressing higher levels of the transgene than the Q129 mice (20). Although the intensities of the truncated bands and the smears were considerably different between Q129 and AT-FL-65Q-150, this may reflect the higher expression levels of mutant DRPLA proteins in AT-FL-65Q-150 and regional differences in expression depending on the promoter driving the transgenes (Q129: own promoter of *DRPLA* gene; ATFL-65Q: prion promoter). The difference in the western blotting patterns detected by AP142 and C580 raises many possibilities, including that a fraction of accumulated mutant DRPLA proteins in the nucleus are truncated at the carboxy terminus. This possibility should be thoroughly investigated employing sensitive procedures including additional antibodies.

Transcriptional down-regulation becomes prominent in an age-dependent manner

As described above, the most fundamental pathological change was the age- and expanded-polyQ-length-dependent NIA of mutant proteins without any obvious neuronal loss, raising the possibility that such an NIA of mutant proteins leads to neuronal dysfunction including synaptic transmissions through transcriptional dysregulations. Thus, we analyzed expression profiles (~11 000 genes) in the brains of the Q129 and non-TG littermates at 4 and 12 weeks of age using GeneChip Mu11K oligonucleotide microarrays (Affymetrix, Santa Clara, CA). To determine how gene expressions are affected as a function of disease duration, we selected dysregulated genes at each age using one-way analysis of variance (ANOVA) with error-weighting. On the basis of our criteria described in Materials and Methods, we detected 54 and 92

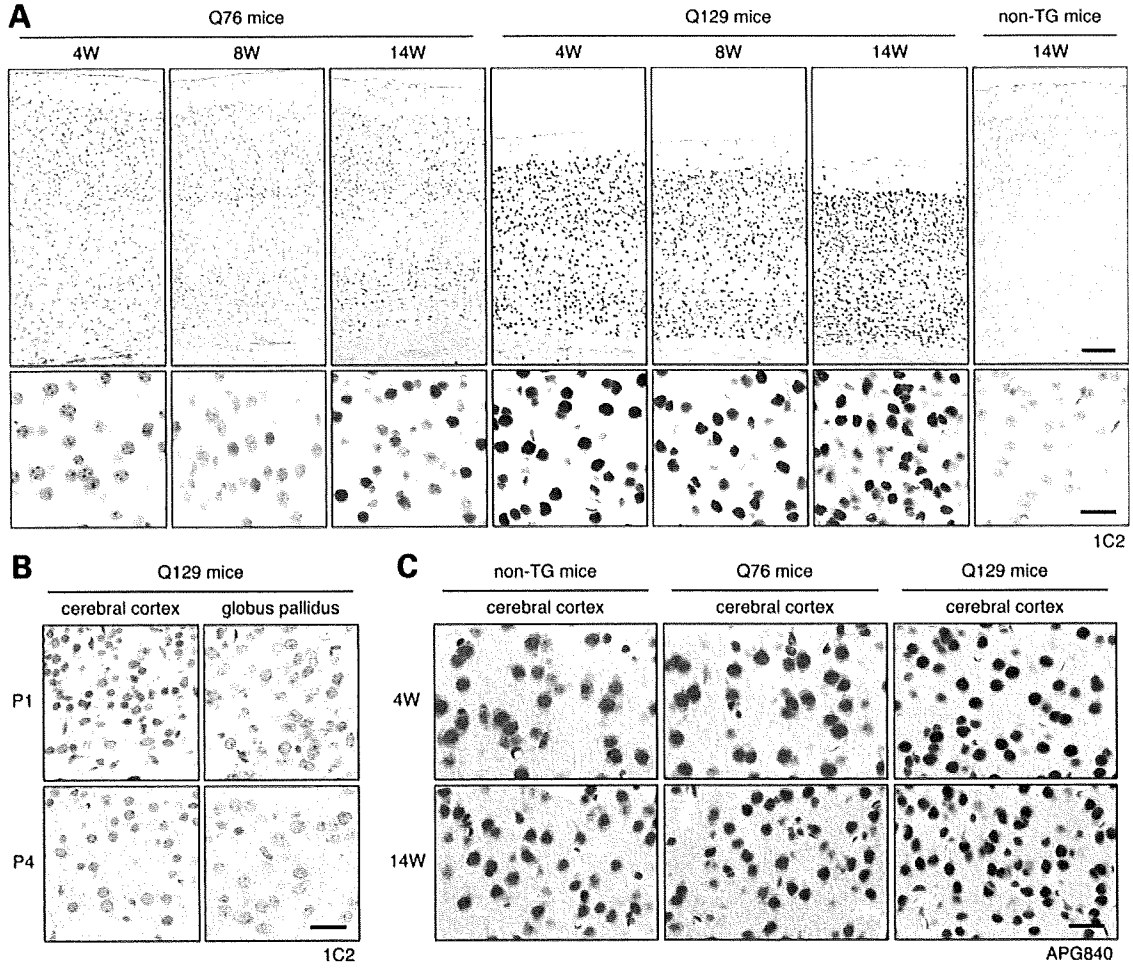

Figure 4. Age- and expanded-polyQ-length-dependent changes in NIA of mutant DRPLA proteins. (**A**) Immunohistochemical analysis of cerebral cortices of the Q76, Q129 and non-TG mice was performed using 1C2. The upper panels show the entire cerebral cortices and the lower panels show cortical layer III. In the Q129 mice (middle panels), the decrease in cortical size was already evident at 4 weeks of age and the cerebral cortex progressively atrophied with age. Neuronal nuclei in all the cortical layers showed intense labeling of expanded polyQ stretches and became gradually packed with age. Age-dependent nuclear atrophy and deformity were also observed (lower panels). There was no obvious neuronal loss in the Q129 mouse brain. In the Q76 mice (left panels), there was no obvious decrease in cortical size. In the lower panels, a gradual increase in the number of neuronal nuclei labeled by 1C2 was observed. Such nuclear labeling became evident particularly in the cortical layers IV and VI. Scale bar = 100 μm for upper panels and 20 μm for lower panels. (**B**) Immunohistochemical analysis of cerebral cortical layer VI and GP of the Q129 mice using 1C2 revealed faint NIA on P4, but not on P1. Scale bar=20 μm. (**C**) Immunohistochemical analysis of cerebral cortical layer III using APG840, an anti-DRPLA protein (atrophin-1) antibody, also revealed polyQ-length-dependent and age-dependent intranuclear accumulation of mutant DRPLA proteins. Scale bar = 20 μm.

down-regulated probe sets, as well as 38 and 20 up-regulated sets at 4 and 12 weeks of age, respectively. The number of down-regulated genes tended to increase with age. We next searched for genes showing age-dependent changes in the levels of expression determined by the two-way ANOVA. We found 46 down-regulated genes (corresponding to 48 probe sets on the microarrays) and 26 up-regulated genes. Interestingly, many of the down-regulated genes were categorized mainly into specific functional molecules, such as neuropeptides, transcriptional factors and signaling molecules (Fig. 6). Although all of the down-regulated genes showed further decreases in expression level with age, the degrees of decrease were different and a limited number of the genes, mainly categorized into neuropeptides, showed a marked decrease (fold change < -1.5) at 4 weeks of age. To determine the relevance of the down-regulated genes to CREB-dependent transcriptional dysregulation, we examined whether these down-regulated genes are candidates for CREB target genes (21,22). We found that 21 of the 46 (46%) down-regulated genes and 17 of the 28 (61%) strongly down-regulated genes (fold change < -1.5; shown in blue in Fig. 6) have cAMP response element (CRE) sites that are conserved between human and rodent orthologs. Among the down-regulated genes, we further confirmed decreased protein levels of arginine vasopressin (Fig. 1F) and kalirin (see Supplementary Material, Fig. S1).

DISCUSSION

Q129 mice as a model to understand the mechanisms of *en masse* expansion or contraction of CAG repeats

We established the Q129 DRPLA transgenic mice by utilizing a unique phenomenon, *en masse* expansion of CAG repeats.

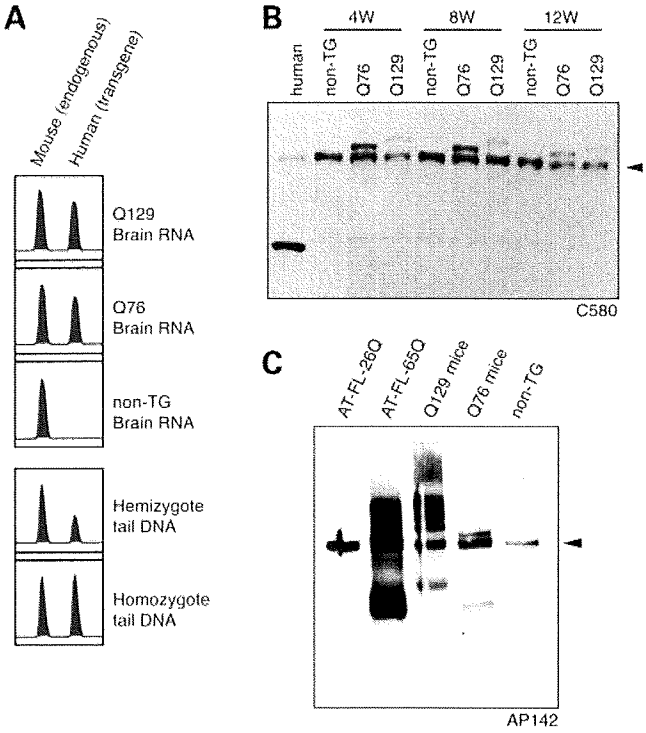

Figure 5. Quantification of mutant DRPLA mRNA levels and western blot analysis of DRPLA proteins in Q129 mouse brains. (**A**) The expression levels of DRPLA mRNAs derived from the transgene and mouse endogenous *DRPLA* gene were quantified by competitive RT–PCR. Considering that the length of the homo-serine stretch in the human *DRPLA* gene is 9 bp longer than that in the mouse *DRPLA* gene, we amplified a segment of DRPLA genomic DNA or cDNAs using flanking primers that completely match both the human and mouse genomic sequences. The validity of the quantitative analysis was confirmed by gene dosage analysis of human mutant transgenes when compared with endogenous mouse *DRPLA* genes. The expression levels of human *DRPLA* gene-derived mRNAs of Q129 and Q76 were determined for each to be 80% of the endogenous mouse DRPLA mRNA level. (**B**) Western blot analysis of total brain homogenates employing C580 revealed two bands corresponding to mouse endogenous (arrowheads) and transgene derived DRPLA proteins in the Q76 or Q129 mice. The lane for human control brain carrying 13 and 9 CAG repeats (lane 1) showed a weak band corresponding to the full-length human DRPLA protein. The intensities of the full-length protein in autopsied brains have been shown to be variable, possibly due to the intrinsic instability of the DRPLA protein, and the identity of the 100-kDa band detected by C580 remains unknown as previously described (17). (**C**) Western blot analysis of nuclear fractions using AP142 showed smears migrating between the stacking gel and the full-length bands. The smaller bands, possibly truncated, with polyQ-length-dependent mobility shifts were observed in Q129 and Q76. As a comparison, other DRPLA transgenic mouse models (20; AT-FL-26Q-84 and AT-FL-65Q-150 at 7.5 months of age) were also analyzed. In the lane for AT-FL-65Q mice, a massive amount of smears as well as truncated proteins with a faster mobility than those in the lane for Q129 mice were observed.

This is the first report of a polyQ model generated by *en masse* expansion. We previously showed age-dependent changes in expanded CAG repeats in somatic tissues as well as intergenerational instabilities of expanded CAG repeats (13). The mechanism of instability has been assumed to be cumulative accumulation of short repeat changes with age, typically one-repeat additions or subtractions. In contrast, *en masse* expansion (Fig. 1A, lane 1) or contraction (Fig. 1A, lane 2) is quite different in terms of the frequency and length of repeat changes. The large intergenerational increase in the CAG repeats to expanded alleles from the intermediate alleles has been observed in a small number of HD or SCA7 patients, and is called the *de novo* expansion (23–25). This phenomenon may be similar to the *en masse* expansion observed in this study. Based on these observations, there seem to be two discrete mechanisms of CAG repeat instability: cumulative accumulation of short repeat changes with age and *en masse* changes occurring spontaneously, but infrequently. Because the mosaic mice were hemizygous, inter-allelic recombination mechanisms are unlikely to be involved. We previously reported a patient with *en masse* expansion of impure CAG repeats in the TBP gene. In this case, inter-allelic recombination events were excluded on the basis of haplotype analysis (26). These intriguing observations suggest that simple intra-allelic rearrangements are involved in the CAG repeat instabilities associated with *en masse* expansions or contractions, which have also been suggested to be involved in somatic instability of minisatellites (27). Taking advantage of the instability of the 129 CAG repeats, we have recently obtained transgenic models carrying 113 or 96 CAG repeats with moderately severe neurological phenotypes (unpublished observation). Thus, transgenic models carrying single copy genes within a full-length genomic context may serve to produce those with variable lengths of expanded CAG repeats.

Q129 mice as an excellent model to understand disease pathogenesis of DRPLA

The Q129 and Q76 mice should be highly valuable for investigating expanded-polyQ-length-dependent effects, because the only difference between the Q129 and Q76 mice is the length of expanded CAG repeats within an identical integration site. The severe neurological phenotypes of the Q129 mice are quite similar to those observed in juvenile-onset DRPLA patients. It should be noted, however, that the phenotypes of Q129 mice were distinct from previously generated mouse models of polyQ diseases. The Q129 mice showed myoclonus, epilepsy and progressive brain atrophy, which are the predominant clinical presentations in DRPLA patients. In contrast, feet clasping observed in R6/2 mice, SCA1 knock-in mice and DRPLA cDNA mice of AT-FL-65Q-150 (19,20,28) was absent in the Q129 mice. Electrophysiological abnormalities have been shown to vary considerably among polyQ models, even among HD yeast artificial chromosome transgenic, HD knock-in and R6/2 mice (29–31), suggesting that the synaptic dysfunctions underlying the distinct phenotypes are dependent on the promoters, copy numbers and the contexts of transgenes. Thus, the Q129 mice harboring a single copy of the full-length human *DRPLA* gene under the control of its own promoter should be highly valuable for investigating the molecular pathogenesis of DRPLA.

NIA of mutant DRPLA proteins is the essential pathophysiologic process

The regional distribution of NIA, particularly that of Q76 mice, is prominent in DRPL systems, the most vulnerable regions in DRPLA patients (1). We have also observed a similar regional distribution of NIA in human autopsied brains (10). In contrast to the Q76 mice, a massive NIA of mutant DRPLA proteins

Probe Set ID	Gene	CRE	Fold Change		Intensity-Q129	
			4W	12W	4W	12W
	Neuropeptide					
M88354_s_at	arginine vasopressin	●	-2.8	-8.7	0.17	0.11
M88355_s_at	oxytocin		-1.9	-5.1	0.32	0.16
X51468_f_at	somatostatin	●	-2.7	-3.0	3.45	2.55
Msa.2612.0_f_at	somatostatin	●	-2.5	-3.0	4.89	3.39
Msa.15880.0_s_at	neuropeptide Y		-1.6	-2.2	3.74	2.50
Msa.512.0_f_at	cholecystokinin	▲	-1.2	-2.0	6.87	3.96
m13227_f_at	preproenkephalin 1	●	-1.4	-1.8	3.00	2.09
	Transcriptional factor					
U29762_s_at	Dbp		-1.1	-3.2	1.28	0.54
m22326-2_s_at	Egr1	●	-1.2	-2.1	2.59	1.89
v00727_s_at	Fos	●	1.0	-2.1	0.68	0.53
x16995_s_at	Nr4a1	▲	-1.2	-2.0	1.60	1.19
Msa.3289.0_s_at	Bhlhb2	▲	-1.2	-2.0	0.76	0.67
Msa.5646.0_s_at	LIM domain only 4	▲	-1.2	-1.8	2.62	2.14
aa183623_s_at	Mef2c	▲	1.0	-1.3	2.46	1.54
aa408983_rc_g_at	Mef2d	▲	-1.0	-1.2	3.23	2.34
	Signaling molecule					
AA673405_rc_at	kalirin, RhoGEF kinase	▲	-1.6	-2.4	1.47	1.01
u05683_s_at	TYRO3 protein tyrosine kinase 3		-1.5	-2.2	1.53	0.98
Msa.1590.0_s_at	protein kinase C, delta		-1.5	-2.2	0.99	0.94
d43796_s_at	Excitatory amino acid transporter 2		1.3	-2.1	0.23	0.13
aa607353_at	Ngef (Ephexin)		-1.4	-1.9	3.45	2.21
Msa.500.0_f_at	S100 calcium binding protein A10 (calpactin)		1.2	-1.5	1.76	1.07
AB006191_at	cornichon homolog 2		-1.1	-1.4	5.54	3.81
aa245242_s_at	MARCKS-like protein		1.0	-1.3	4.81	2.16
x61432_f_at	calmodulin 1		1.1	-1.2	12.98	11.11
	Vesicular transport					
d83277_at	RAB33A, member of RAS oncogene family		-1.1	-1.8	2.29	1.18
M62418_s_at	adaptor protein complex AP-1, sigma 1	▲	-1.2	-1.5	4.61	4.07
D86214_s_at	Ca<2+>dependent activator protein for secretion		-1.1	-1.5	2.73	1.96
D83206_s_at	vesicular membrane protein p24		-1.1	-1.4	4.23	3.20
Msa.17373.0_f_at	synuclein, alpha		1.2	-1.3	1.36	1.03
	Cytoskeleton and Structual molecule					
x07215_s_at	proteolipid protein (myelin) 1		-1.0	-1.5	11.32	5.30
j04181_f_at	actin, beta, cytoplasmic		-1.1	-1.5	2.11	1.66
U19582_s_at	claudin 11	▲	1.0	-1.4	6.27	2.60
m13444_s_at	tubulin, alpha 4		-1.0	-1.4	6.14	5.34
AA590859_f_at	actin, beta, cytoplasmic		-1.0	-1.3	5.02	3.77
Msa.1236.0_f_at	thymosin, beta 4, X chromosome		1.1	-1.2	11.82	10.32
Msa.16998.0_f_at	stathmin 1		1.1	-1.2	15.32	12.45
	Cell cycle					
Msa.15616.0_s_at	cyclin D2	▲	1.1	-1.9	0.30	0.18
C78067_rc_at	Bub3	▲	1.2	-1.8	0.21	0.11
	Protein folding					
Msa.32815.0_s_at	DnaJ (Hsp40) homolog, subfamily B, member 7		1.1	-1.7	0.35	0.21
C79184_rc_s_at	karyopherin (importin) alpha 2		1.1	-1.2	4.57	3.06
	Cholesterol biosynthesis					
aa275198_s_at	HMG-CoA synthase	●	-1.1	-1.7	3.21	1.88
D29016_s_at	farnesyl diphosphate farnesyl transferase 1	▲	1.1	-1.4	1.90	1.58
	Metabolic enzyme					
Msa.34555.0_s_at	ATPase, Na+/K+ transporting, alpha 1 polypeptide	●	1.2	-4.2	0.37	0.65
Msa.3814.0_s_at	Serpinb1a		1.3	-1.9	0.39	0.18
k00811_s_at	carbonic anhydrase 2		-1.2	-1.7	5.74	4.14
	Miscellaneous					
aa289338_s_at	cAMP-regulated phosphoprotein 19	▲	-1.5	-2.5	1.22	0.90
aa409164_rc_s_at	RIKEN cDNA E130012A19 gene	▲	-1.5	-2.2	1.14	0.71
AA250009_s_at	schwannomin interacting protein 1		-1.1	-1.3	3.54	2.59

Figure 6. Expression profiles in brains of the Q129 mice compared with those in the non-TG littermates. The fold changes of the genes in the Q129 mice ($n = 3$) compared with those in the non-TG mice ($n = 3$) and the intensities in the Q129 mice at 4 or 12 weeks of age are summarized, which were calculated with the Rosetta Resolver (Ratio Experiment) using the Affymetrix-Default Ratio Builder. Fold changes are shown as columns of blue, light blue, yellow and pink indicating fold changes of < -2.0, -1.5, -1.2 and others, respectively. Filled circles: CREB targets described by Mayr and Montminy (21). Filled triangles: putative CREB targets classified as conserved CRE (22). Genes of neuropeptides in the Q129 mice, including vasopressin, oxytocin, somatostatin and neuropeptide Y, were strongly down-regulated even at 4 weeks of age. The latest description of each gene was obtained from the Probe Set at the NetAffx Analysis Center (www.affymetrix.com).

occurred throughout the Q129 mouse brain. It is noteworthy that NIA was not present on P1 even in the Q129 mice, but was the earliest change among any other abnormalities including neurological phenotypes and electrophysiological abnormalities. It should also be mentioned that the distribution of NIA far exceeded the DRPL systems. This may provide an explanation as to the controversial issue that the neuronal loss involving DRPL systems alone cannot account for the broad clinical manifestations of DRPLA. In particular, massive NIA observed in the cerebral cortex may account for the development of dementia, myoclonus and epilepsy. Taken together, these observations strongly suggest that NIA plays essential roles in the pathogenesis of DRPLA.

The mechanisms underlying the regional specificity of NIA of mutant DRPLA proteins, however, remain to be elucidated. Interestingly, NIA of mutant DRPLA proteins appeared after P4 even in the Q129 mice, whereas the transcript is abundantly expressed as early as embryonic day 5 and thereafter (32).